Nuclear structure investigation of odd-odd $^{92-98}$Y nuclei

Falih H. Al-Khudair and Musa M. Mahdi
Department of Physics, College of Education for Pure Sciences, University of Basrah, Basrah 61004, Iraq

(Received 29 August 2021; revised 10 April 2023; accepted 7 June 2023; published 5 July 2023)

The structure of the energy states and its decay properties in odd-odd $^{92-98}$Y isotopes have been investigated via the framework of the interacting boson fermion-fermion model (IBFFM-1). To complete the system of the model, the nuclear structure of the even-even $^{90-96}$Sr isotopes has been described from the IBM-1 as a core part. The nuclear structure of odd-Z $^{91-97}$Y and odd-N $^{91-97}$Sr isotopes is studied in the IBFM-1. The single-, quasi-particle energies and the occupation of valence protons (neutrons) $1f_{7/2}$, $1f_{5/2}$, $2p_{3/2}$, $2p_{1/2}$ and $1g_{9/2}$ ($2d_{5/2}$, $2d_{3/2}$, $1g_{7/2}$, $3s_{1/2}$ and $1h_{11/2}$) single-particle orbitals have been calculated. Angular momentum assignments for some uncertain experimental levels made based on the model calculations. The model calculations gave consistent and detailed description of the nuclear structure of even-even, odd-A, and odd-odd Sr and Y of this mass region nuclei.

DOI: 10.1103/PhysRevC.108.014305

I. INTRODUCTION

Shape coexistence and intruder orbitals are quite common phenomena in the $Z \approx 40$ nuclei [1–3]. The neutron-rich $^{90-98}$Sr and $^{91-98}$Y nuclei, for example, show a sudden beginning of deformations between neutron numbers $N = 52$, with spherical shapes, $N = 58$, with nearly spherical shapes, and $N = 59$, where the ground states are deformed [4,5]. In $A \approx 100$ region, the neutron-rich yttrium isotopes are of particular interest because they are located between to some extent spherical and a well-deformed region [6–12]. This is noticeable for the isotopic chains near $Z \approx 40$, namely Nb, Zr, Sr, and Y nuclei [13–15]. The nuclear structure with $N \leqslant 58$ can be understood in terms of the shell model for spherical nuclei (the lighter isotopes up to $N = 58$ hold a stable spherical shape), whereas the $N \approx 60$ isotones are deformed in their ground states [16]. Thus, an important question arises about the behavioral nature of the last $N = 59$ isotones for ^{97}Sr and ^{98}Y isotopes, which are the link between the spherical and deformed regions and for which shape coexistence is expected. In this mass region, the $\pi g_{9/2}$ and $\upsilon h_{7/2}$ orbitals are located near the Fermi surface and play a major role in the bands structure of this region [17].

Several theoretical and experimental works were carried out investigate the nuclear structure for Sr and Y isotopes. Tel *et al.* [18] have theoretically calculated the nuclear neutron and proton densities and binding energies of the Sr isotopes ($A = 84$–96). They used the Skyrme-Hartree-Fock (SHF) parameters to investigate the ground-state properties and the nuclear shape. Clément and Zielińska [19] discussed the shape coexistence in the nuclear structure of ^{96,98}Sr isotopes. The results showed that the shape shift at $N = 60$ leads to the coexistence of a highly deformed prolate, and a spherical configuration in $N = 98$ with low configuration mixing.

Nomura *et al.* [20] studied the shape coexistence in the $^{92-108}$Sr isotopes within the IBM model with microscopic input from the self-consistent mean-field model based on the Gogny-D1M energy density functional. They have mapped the deformation PES in the quadrupole deformation parameters (β, γ). A clear coexistence is found between very weakly oblate (up to $N = 58$) and strongly prolate-deformed shapes (starting at $N = 59$). Régis *et al.* [21] showed that the results of the sudden change of shape for Sr isotopes near $N = 60$ resulted from the excitation of many protons in the $g_{9/2}$ orbit. The Monte Carlo shell-model results have been done without truncation on the occupation numbers of the orbits with eight protons and eight neutron orbits. Wimmer *et al.* [22] investigated the presence of spherical-deformed shape transition for neutron-rich Sr isotopes. Monte Carlo shell model calculation for ^{95}Sr nucleus predicted the coexistence shape of the ground band, prolate excited intruder states, and a triaxial deformed band built on the low-lying $7/2^+$ state.

Esmaylzadeh *et al.* [5] used the Lohengrin spectrometer to measure delayed γ rays from neutron-rich ^{97}Sr fission fragments and measured several lifetimes of excited states using fast-timing technique. The experimental results are compared with a boson-fermion model based on the microscopic energy density functional. They concluded that the ^{97}Sr nucleus is exactly at the spherical-deformed limit. Cruz *et al.* [23] based on the idea of a dramatic ground-state transition from spherical (near) below $N = 60$ in Sr and Zr nuclei to deformed shapes in heavy isotopes. The single-particle structure of $^{95-97}$Sr, that approximates the ground-state transition at ^{98}Sr, was investigated using (d, p) interaction in inverse kinetics. The experimental results were compared with shell model calculations and they showed that the ground state is weakly deformed in the ^{96}Sr nucleus and that the first two excited levels overlap significantly, while we find that the ground state of ^{97}Sr nucleus has a different structure. The single-particle and collective structure in Sr ($N = 50$–58) isotopes have been investigated using shell model [24]. The energy spectra and transitions rates of these isotopes were well described in this work.

Cruz *et al.* [25] used the reactions of a single neutron striping 2H (^{94,95,96}Sr,t) to study the nuclear structure of the Sr nuclei. The experimental results were compared with the shell model calculations and the results were encouraging, as the two-level mixing analysis of the levels 0^+ in ^{94}Sr indicated a strong mixing of two shapes. They showed that the shape transition indicators are clear before $N = 60$ due to the complexity in the configuration of the ground state of the ^{96}Sr nucleus, and that the agreement with the shell model was less good in the ^{95}Sr nucleus.

Mei *et al.* [26] solved a five-dimensional collective Hamiltonian (5DCH) with selected parameters from both relativistic mean-field (RMF) and nonrelativistic SHF to study the change of nuclear structure in Sr and Zr isotopes. The excitation energies, isotopic displacements, and quadrupole electric transition strengths were calculated and compared with the corresponding experimental data.

The present work has been organized as follows. In Sec. II we describe the procedure to construct the IBFFM Hamiltonian including the Hamiltonian of even-even, odd-*A*, and odd-odd nuclei. The results for low-lying spectra in the even-even Sr, odd-*N* Sr, and odd-*Z* Y nuclei are reviewed and discussed in Sec. III, followed by the results of the spectroscopic calculations for the odd-odd Y nuclei. Finally, in Sec. VI we summarize our calculations.

II. THEORETICAL FRAMEWORK

A. Hamiltonian

In order to investigate the IBFFM Hamiltonian in the bosons and fermion interactions space, we can trace the success of the model in describing the nuclear structure of the even-even and odd-even nuclei. The collective features in even-even isotopes have been previously investigated in the first version of IBM-1 with one kind of bosons [27–29]. For odd-mass-number nuclei, the model is expanded into a fermion boson model [30,31]. For more complex nuclear structure, the model was extended to describe odd-odd nuclei and called the interacting boson fermion-fermion model (IBFFM) [32–34]. The writing of the IBFFM Hamiltonian depends on the structure of the core. Here the sd form has been used to build the model Hamiltonian [35].

$$H = H_B + H_F^{\upsilon} + H_F^{\pi} + H_{\mathrm{BF}}^{\upsilon} + H_{\mathrm{BF}}^{\pi} + V_{\mathrm{Res}}. \tag{1}$$

The H_B represents the IBM Hamiltonian for the even-even core nucleus. The H_F^{ρ} and H_{BF}^{ρ} ($\rho = \upsilon, \pi$) represent the two terms of the IBFM Hamiltonian for the odd-neutron and odd-proton nuclei, respectively. The last term (V_{RES}) denotes the residual proton-neutron interaction. Starting with general IBM-1 Hamiltonian for N-boson system, which is written as [30]

$$H_{\mathrm{IBM}} = \sum_{i=j}^{N} \epsilon_i + \sum_{i<j}^{N} V_{ij}, \tag{2}$$

where ϵ_i and V_{ij} represent the one-boson energy and the boson-boson interaction energy. The Hamiltonian in Eq. (2) has been written in the multipole expansion form as follows [27–29,36]:

$$H_B = \epsilon_d \hat{n}_d + a_0 \hat{P}.\hat{P} + a_1 \hat{L}.\hat{L} + a_2 \hat{Q}.\hat{Q} + a_3 \hat{T}_3.\hat{T}_3 + a_4 \hat{T}_4.\hat{T}_4. \tag{3}$$

The ϵ_d and $\hat{n}_d$ are the energy and the number operator of the d boson, respectively. $\hat{L} = \sqrt{10}\hat{T}_1$ is the angular momentum operator. The second and fourth terms represent the paring and quadrupole operators, where

$$\hat{P} = \tfrac{1}{2}[(\tilde{d} \cdot \tilde{d}) - (s \cdot s)] \tag{4}$$

$$\hat{Q} = [d^{\dagger} \times s + s^{\dagger} \times \tilde{d}]^{(2)} - \chi[d^{\dagger} \times \tilde{d}]^{(2)}, \tag{5}$$

$\hat{T}_{\ell} = (d^{\dagger} \times \hat{d})^{(\ell)}$ ($\ell = 3$ and 4) represent the octopole and hexadropole operators, respectively.

In the IBFM model, the collective degrees of freedom are described by boson operators. The Hamiltonian contains a part that describes the bosons(H^B), a part that describes the fermions(H^F), and a part that describes the interaction between the bosons and fermions (V^{BF}) [30,37]:

$$H^{\mathrm{IBFM}} = H^B + H^F + V^{\mathrm{BF}} \tag{6}$$

the fermion Hamiltonian H^F consists of one-body terms (i.e., quasiparticle).

$$H^F = \sum_i \epsilon_i n_i, \tag{7}$$

where ϵ_i and n_i are the quasiparticle energy of the ith orbital and the fermion number operator, respectively. The energies of the quasiparticle have been calculated by solving BCS equation [38]

$$\epsilon_i = \sqrt{[(E_i - \lambda)^2] + \Delta^2]} \tag{8}$$

$$\upsilon_i^2 = \frac{1}{2}\left[1 - \frac{(E_i - \lambda)}{\epsilon_i}\right] \tag{9}$$

$$u_i = \left(1 - \upsilon_i^2\right)^{1/2}. \tag{10}$$

Where λ, Δ, E_i, and υ_i^2 represent the Fermi energy, paring gap, single-particle energies and occupation probabilities, respectively. The last term in Eq. (6) represents the interaction between the odd fermion and the bosons of the core nucleus, it is rather intricate, but has been shown to be dominated by the following three parts [31]:

$$V^{\mathrm{BF}} = \sum_{jj'} \sum_{j} A_j[(d^{\dagger}\tilde{d})^{(2)}(a_j^{\dagger}\tilde{a}_j)^{(0)}] + \Gamma_{jj'}\left[Q_{jj'}^{(2)}(a_j^{\dagger}\tilde{a}_j)^{(2)}\right]_0^{(0)} + \sum_{jj'j''} \Lambda_{jj'}^{j''} : [(d^{\dagger}\tilde{a}_j)^{j''}(a_{j'}^{\dagger}\tilde{d}_j)^{(j'')}]_0^{(0)}. \tag{11}$$

The first term is a monopole interaction that depends on the number of d bosons and the effect on the spectrum that compresses or expands it without changing the order of states. The second term symbolizes the direct component of the quadrupole interaction between the single fermion and bosons. However, this term gives rise to a splitting but without shifting the boson multiplets [37]. The last term is the exchange interaction of the quasiparticle with one of two fermions forming a boson, which brings the Pauli exclusion

principle and gives rise to splitting and a shift of the multiplets. The remaining parameters in Eq. (11) can be related to the BCS occupation probabilities of the single-particle orbitals:

$$\begin{aligned}\Gamma_{jj'} &= \sqrt{5}\Gamma_0(u_j u_{j'} - \upsilon_j \upsilon_{j'})Q_{jj'};\\ \Lambda_{jj'}^{j''} &= -\sqrt{5}\Lambda_0[(u_{j'}\upsilon_{j''} + \upsilon_{j'}u_{j''}Q_{j'j''}\beta_{j''j})\\ &\quad + (u_{j'}\upsilon_{j''} + \upsilon_{j'}u_{j''}Q_{j'j}\beta_{j'j''})]/\sqrt{2j''+1}\\ A_j &= -A_0\sqrt{2j+1}\end{aligned} \tag{12}$$

in which $Q_{j'j''}$ is the single-particle matrix element of the quadruple operator and:

$$\beta_{jj'} = (u_j \upsilon j' + \upsilon_j u_{j'})Q_{jj'}. \tag{13}$$

The last term V_{RES} in Eq. (1) is the residual interaction between the odd proton and the odd neutron, which takes the form [39],

$$V_{\mathrm{RES}} = V_q Q_p \cdot Q_n + V_s \sigma_p \cdot \sigma_n. \tag{14}$$

As in the Hamiltonian model, the structure of odd-odd nuclei associated with proton and neutron quasiparticles in the unique-parity orbitals coupled to the even-even core. Although the quadrupole-quadrupole interaction is the dominant component in the residual interaction, $\pi - \nu$ residual interaction plays a relatively minor role because such interactions are already included in the particle-boson interactions. On the other hand, the spin-spin interaction has effects on the sequence of the lowest-energy levels [40].

B. A procedure for building the IBFFM-1 Hamiltonian

In the first step of the IBFFM-1 calculations, the boson core should be fitted to the low-lying levels in the even-even $^{90-96}$Sr, and then carry out the $B(E2)$ calculation. In the second step, single-particle energies and occupation probabilities of the odd nucleon are calculated using BCS theory [38]. Optimal values of the boson-fermion interaction Γ_ρ, Λ_ρ, and $A_\rho(\rho = \pi, \nu)$ parameters have been chosen in the calculation of the positive parity states of $^{91-97}$Sr nuclei and the negative parity states of $^{91-97}$Y nuclei.

In the third step, with the same parameters values used in core and odd-A as well as the parameters of the residual proton-neutron interaction the low-lying spectra and electromagnetic transition probabilities for odd-odd Y nuclei have been investigated using IBFFM code written by Scholten [41]. The full energy spectrum is calculated by diagonalizing the Hamiltonian in Eq. (1) in the following basis state:

$$|(\hat{j}_\pi \hat{j}_\nu)j_{\pi\nu}, n_d \nu I; J\rangle, \tag{15}$$

where $(j_\pi, j_\nu)j_{\pi\nu}$ represents the state with quasiproton (j_π) and quasineutron (j_ν) coupled to the angular momentum $j_{\pi\nu}$. $|n_d \nu I\rangle$ represent the standard core basis states with n_d d boson and $n_s = N - n_d$ coupled to angular momentum I. The total angular momentum of odd-odd state J comes from the coupling $j_{\pi\nu}$ and I. The IBFFM wave functions are expressed as follows [42]:

$$|J_r\rangle = \sum \zeta^{(J_r)}_{(j_\pi j_\nu)j_{\pi\nu}, n_d \nu I} |(\hat{j}_\pi, \hat{j}_\nu)j_{\pi\nu}, n_d \nu I; J\rangle. \tag{16}$$

TABLE I. The parameters of the model Hamiltonian in Eq. (3) used for the description of the $^{90-96}$Sr nuclei, all parameters are given in MeV, except χ, which is dimensionless.

nucleus	N	ϵ_d	a_0	a_1	a_2	a_3	χ
^{90}Sr	6	0.695	0.002	0.011	0.000	0.035	0.000
^{92}Sr	7	0.695	0.002	0.011	0.000	0.035	0.000
^{94}Sr	8	0.725	0.002	0.018	−0.001	0.035	−0.003
^{96}Sr	9	0.750	0.0026	0.012	−0.001	0.010	−0.003

III. CALCULATION AND DISCUSSION

A. Even-even $^{90-96}$Sr nuclear structure

In this section, in short, we will discuss relevant calculations for the even-even $^{90-96}$Sr nuclei. The Sr isotope with $Z = 38$ and neutron number vary from 52–58. Relative to the $Z = 28$ and $N = 50$ close shells, these nuclei have $N_\pi = 5$ and N_ν goes from 1–4. All bosons are particle type. The values of parameters of the model Hamiltonian used to calculate the energy levels are given in Table I. The values were chosen based on the shape of the nuclei, depending on the ratio $E4_1^+/E2_1^+$, as well as the position of 0_2^+ state. Taking into account the deformations that occur in the nuclear structure, the quadrupole-quadrupole interaction has been added to Hamiltonian of the ^{94,96}Sr isotopes. The comparison between the calculated energy levels and the available experimental [43] is shown in Figs. 1 and 2. Examining the calculated results, there is reasonable agreement with the available data.

For ^{90}Sr isotope, the energy ratio $E4_1^+/E2_1^+ = 1.99$ and 2.11 in the experimental data and model calculation, respectively, suggests vibrational shape. The ground state has a spherical pattern with a 2_1^+ excitation at 0.831 MeV, which is in good agreement with IBM-1 results at 805 MeV. On the other hand, the energy of $4^+_{2\mathrm{phonon}}$ state is equal to 1.655 and 1.706 MeV in the experimental and model results, respectively. Theoretically, the energy of the $I^+ = 0^+_{i=2,3,4}$ is

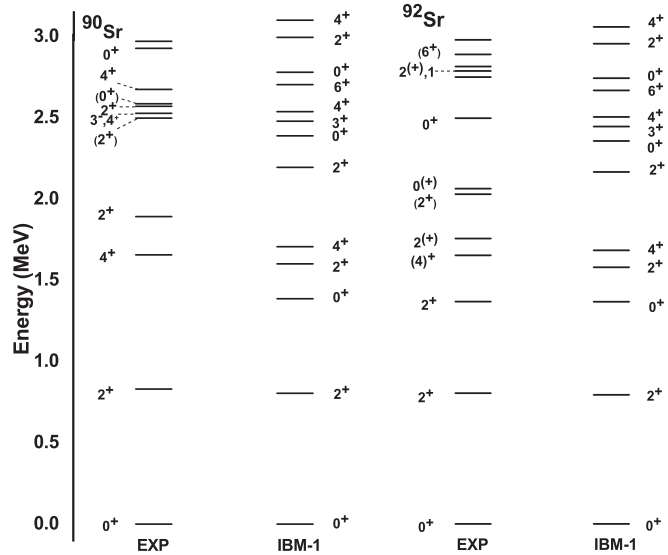

FIG. 1. Calculated and observed energy spectra [43] for ^{90,92}Sr isotopes.

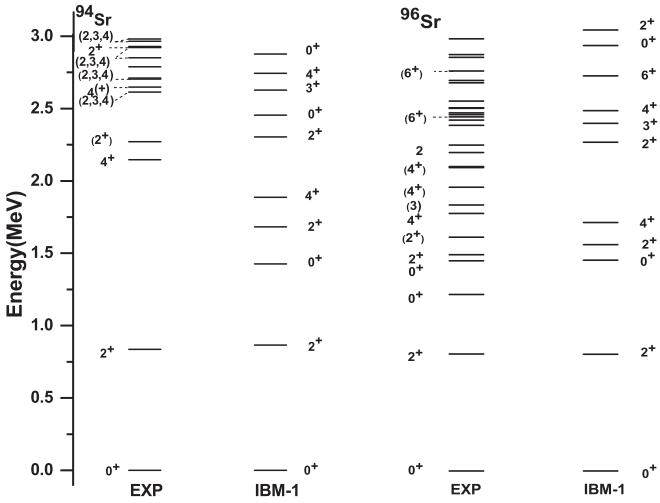

FIG. 2. Same as Fig. 1 but for ^{94,96}Sr isotopes.

equal to 1.386, 2.388, and 2.780 MeV, while there are two 0^+ states at 2.674 MeV with $I^\pi = (0^+)$ and 2.971 MeV with certain $I^\pi = 0^+$ in the experimental data. However, the ^{96}Sr isotope has a 0_2^+ state at 1.229 MeV. The excited states at 2.497 (2^+) and 2.586 MeV 2^+ in the experimental data were assigned theoretically to $I^\pi = 2^+$ at 2.195 and 2.995 MeV, respectively. The 3^-, 4^+ state at 2.527 MeV in the experimental data is close to the 4_2^+ state at 2.538 MeV.

In ^{92}Sr nucleus, there are two 2^+ states above 814 KeV, one at 1.385 MeV with 2^+, which was considered as intruder state [44]. The other state at 1.778 MeV 2_2^+ in good agreement with calculated state at 1.599 MeV. Moreover, it will be interesting to see the position of 4_1^+ state at 1.673 MeV close to the calculated one at 1.704 MeV.

The experimental level at 2.820 MeV has possible [$I = 2^{(+)}$, (1)], which is close to the calculated $I = 2_4^+$ state at 2.991 MeV. The third 0^+ state in ^{92}Sr isotope has been calculated to be about 300 KeV higher than an experimental one. The first 6_1^+ has been calculated to be about 400 KeV lower than the experimental state. The present value is consistent with the shell model calculation [45].

Experimental and calculated level energies in ^{94}Sr were compared in Fig. 2. The first four levels in the ground-state band were well reproduced. The level at 2.614 MeV has possible (2,3,4) assignments close to the calculated 3_1^+ state at 2.628 MeV. On the other hand, the closed-shell model in Ref. [44] estimated this state 3_1^+ at 2.649 MeV instead of $4^{(+)}$ as shown in the spectrum depending on the calculated $B(E2)$, $B(M1)$, and mixing ratios, by decaying to the 2_1^+ and 4_1^+ states

Figure 2 presents a more detailed comparison between experimental and calculated energy levels in ^{96}Sr. In this isotope, two valence neutrons can occupy the $g_{7/2}$ or $s_{1/2}$ orbitals. The low-lying levels in ^{96}Sr are probably dominated by proton excitations, i.e., promoting a pair of $p_{3/2}$ protons into the $g_{9/2}$ shell [46]. The ground band has a spherical pattern with a $2^+_{1\text{phonon}}$ excitation at 815 KeV, which agrees well with IBM-1 result at 813 KeV. The 0^+ state at 1.465 MeV and 2^+ state at 1.628 MeV were considered as intruder states (for more detail about these states see Refs. [44,47]). The model calculated 3_1^+ at 2.421 MeV in agreement with the state at 2.407 MeV which has no spin assignment. The sequence of levels in the ground-state band is well represented.

B. Odd-neutron $^{91-97}$Sr nuclear structure

We have selected the $^{91-97}$Sr nuclei to be particle neutron nuclei concerning the even-even $^{90-96}$Sr core nuclei, respectively. The positive-parity states of $^{91-97}$Sr are based on the orbits configuration in the $Z = 50$–82 region. There is a single-particle orbital ($\upsilon h_{11/2}$) of negative parity available to the odd-neutron in the major shell and four positive-parity orbitals $1g_{7/2}$, $2d_{5/2}$, $2d_{3/2}$, and $3s_{1/2}$. Because of the smallness of the single-particle energy of the $d_{5/2}$ and $g_{7/2}$ orbitals, the (3–5) valance neutrons in $^{91-97}$Sr at most occupy the $d_{5/2}$ and $g_{7/2}$ orbitals, which means a greater contribution from these orbitals to composite the wave function of the states.

To calculate the energy levels, we have taken into account all these neutron orbitals as listed in Table II. Single-particle energies have been taken from Ref. [48]. The quasiparticle energies and occupation probabilities were calculated from the BCS theory with the energy gap taken to be $\Delta = 12/\sqrt{A}$ MeV. All the quasiparticle energy values and occupation probabilities calculated from BCS theory for these nuclei are kept unchanged for the odd-A nuclei and the corresponding odd-odd nuclei.

The boson-fermion interaction strengths are determined to reproduce the low-lying energy spectrum as well as the energy

TABLE II. Single-particle, quasiparticle energies (in MeV), occupation probabilities and parameters in boson-fermion interaction (in MeV) for $^{91-97}$Sr isotopes.

	^{91}Sr			^{93}Sr			^{95}Sr			^{97}Sr		
	E	ϵ	υ^2	E	ϵ	υ^2	E	ϵ	υ^2	E	ϵ	υ^2
$2d_{5/2}$	−0.119	0.806	0.395	−0.108	0.962	0.627	−0.098	1.269	0.767	−0.089	1.593	0.826
$2d_{3/2}$	3.248	3.623	0.012	3.210	3.211	0.021	3.174	2.805	0.038	3.138	2.500	0.062
$1g_{7/2}$	1.552	2.002	0.040	1.539	1.682	0.083	1.526	1.429	0.169	1.513	1.334	0.289
$3s_{1/2}$	2.193	2.603	0.023	2.177	2.242	0.045	2.162	1.910	0.086	2.147	1.701	0.148
$1h_{11/2}$	2.589	2.983	0.018	2.583	2.617	0.033	2.576	2.265	0.059	2.570	2.021	0.099
Γ		0.390			0.290			0.990			1.090	
Λ		0.580			0.890			2.990			2.890	
A_0		−0.105			−0.105			−0.710			−0.710	

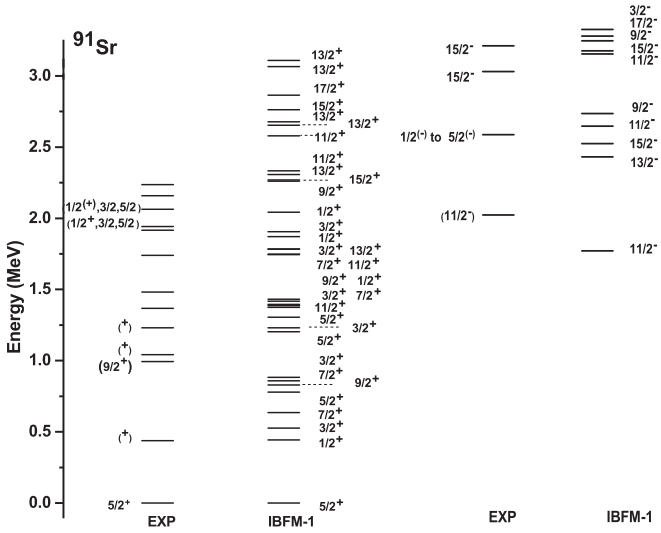

FIG. 3. Same as Fig. 1 but for ^{91}Sr isotope.

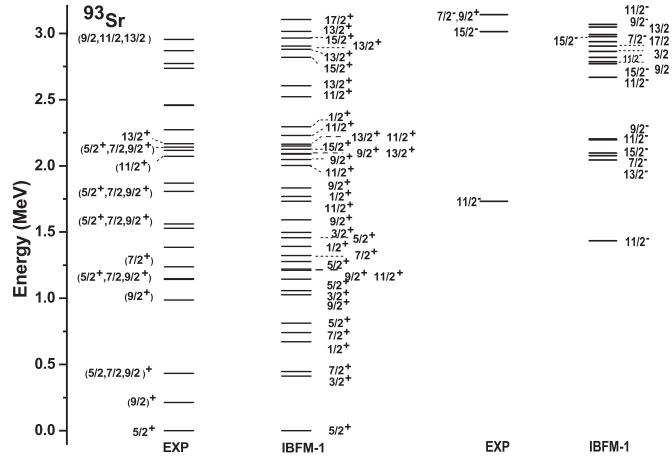

FIG. 4. Same as Fig. 1 but for ^{93}Sr isotope.

difference between the lowest states of each parity. All the strength of the parameters gradually changes with neutrons number, due to the increase in the quasiparticle energies. The Γ_υ has to be increased to lower the energy of the first $3/2^+$ and $7/2^+$ states in ^{93}Sr. The monopole interaction strength has been employed to stretch somewhat the spectrum in ^{95,97}Sr. The obtained values are listed in Table II.

The positive-parity states of the ^{91}Sr isotope have been shown in Fig. 3, in comparison with experimental data [43]. The model calculations give several predictions. The ground state is based on the $d_{5/2}$ quasiparticle state. This pattern might be associated with filling the $\upsilon g_{9/2}$ configuration, which affects the neutron quasiparticle positions via a proton-neutron interaction [49]. The main component of the ground state $5/2^+$ is dominated by the single-quasiparticle state $\upsilon d_{5/2}$ more than 95%. The first excited level $3/2^+$ is at higher energy in IBFM-1 calculation. The calculated $9/2^+_1$ state at 0.830 MeV is close to the experimental level at 0.994 MeV. It is mainly described by $\upsilon d_{5/2}$ as $1\%g_{7/2} + 93\%d_{5/2} + 1\%d_{3/2} + 5\%s_{1/2}$, this compatible with the shell model calculations in Ref. [45]. The model calculation has predicted $9/2^+_2$, $1/2^+_2$, $11/2^+_2$, and $13/2^+_1$ states at 1.417, 1.432, 1.749, and 1.785 MeV, respectively. Major components in the IBFM-1 wave functions for some levels are

$$
\begin{aligned}
|3/2^+_1\rangle &= 89.84\%|2^+_1 \otimes d_{5/2}\rangle + 4.76\%|0^+_1 \otimes d_{3/2}\rangle \\
&\quad + 3.84\%|2^+_1 \otimes g_{7/2}\rangle + \cdots \\
|5/2^+_1\rangle &= 94.90\%|0^+_1 \otimes d_{5/2}\rangle + 3.18\%|2^+_1 \otimes s_{1/2}\rangle \\
&\quad + 1.03\%|2^+_1 \otimes g_{7/2}\rangle + \cdots \\
|7/2^+_1\rangle &= 69.11\%|0^+_1 \otimes g_{7/2}\rangle + 23.41\%|2^+_1 \otimes d_{5/2}\rangle \\
&\quad + 6.74\%|2^+_1 \otimes d_{3/2}\rangle + \cdots \\
|9/2^+_1\rangle &= 92.41\%|2^+_1 \otimes d_{5/2}\rangle + 4.88\%|4^+_1 \otimes s_{1/2}\rangle \\
&\quad + 1.43\%|2^+_1 \otimes g_{7/2}\rangle + \cdots \\
|11/2^+_1\rangle &= 82.37\%|2^+_1 \otimes g_{7/2}\rangle + 9.53\%|4^+_1 \otimes d_{3/2}\rangle \\
&\quad + 7.47\%|3^+_1 \otimes d_{5/2}\rangle + \cdots
\end{aligned}
$$

The calculated energy levels of ^{93}Sr isotope are shown in Fig. 4. The model fails to reproduce the observed low-lying uncertain $(9/2)^+_1$ state at 0.213 MeV. Theoretically, the $3/2^+_1$ state at 0.413 MeV is the first excited state. The second excited state at 0.433 MeV with uncertain $(5/2, 7/2, 9/2)^+$ is close to the calculated $7/2^+_1$ state at 0.447 MeV. The orbital $\upsilon g_{7/2}$ quasiparticle dominated more than 95% of the wave function. The next higher-lying doublet $(5/2^+, 7/2, 9/2^+)$ at 1.143 and 1.148 MeV have been reproduced in the IBFM-1 calculations at 0.812 and 1.145 MeV with $j = 5/2^+_{2,3}$, respectively. Another higher-lying doublet has uncertain $(5/2^+, 7/2, 9/2^+)$ assignment at 1.562 and 1.808 MeV are close to $j = 5/2^+_4$ and $j = 9/2^+_4$ at 1.277 and 1.834 MeV, respectively. The level $11/2^+$ at 2.072 MeV has been identified with the $11/2^+_3$ state at 2.003 MeV. The model wave functions of some levels are

$$
\begin{aligned}
|3/2^+_1\rangle &= 95.91\%|2^+_1 \otimes d_{5/2}\rangle + 2.63\%|2^+_1 \otimes s_{1/2}\rangle \\
&\quad + 1.07\%|2^+_1 \otimes g_{7/2}\rangle + \cdots \\
|5/2^+_1\rangle &= 97.35\%|0^+_1 \otimes d_{5/2}\rangle + 1.68\%|2^+_1 \otimes s_{1/2}\rangle \\
&\quad + 0.70\%|2^+_1 \otimes g_{7/2}\rangle + \cdots \\
|7/2^+_1\rangle &= 95.20\%|0^+_1 \otimes g_{7/2}\rangle + 4.39\%|2^+_1 \otimes d_{3/2}\rangle \\
&\quad + 0.32\%|2^+_1 \otimes d_{5/2}\rangle + \cdots \\
|9/2^+_1\rangle &= 93.51\%|2^+_1 \otimes d_{5/2}\rangle + 3.95\%|4^+_1 \otimes s_{1/2}\rangle \\
&\quad + 1.99\%|2^+_1 \otimes g_{7/2}\rangle + \cdots \\
|11/2^+_1\rangle &= 93.61\%|2^+_1 \otimes g_{7/2}\rangle + 6.28\%|4^+_1 \otimes d_{3/2}\rangle \\
&\quad + 0.10\%|5^+_1 \otimes s_{1/2}\rangle + \cdots
\end{aligned}
$$

As one sees from the comparison between the theoretical and experimental low-energy spectrum for the ^{95}Sr nucleus in Fig. 5, the description of the positive-parity states is generally well. The second excited $(7/2^+_1)$ state at 0.556 MeV with $E_\gamma = 0.204$ MeV by $E2$ transition to $3/2^+$ is close to the calculated state at 0.410 MeV. Experimentally, the level at 0.681 MeV has possible $j = 3/2^+, 5/2^+$ assignments. It is close to the $3/2^+_2$ state at 0.625 MeV in our calculations. The structure of wave function for this state is $40\%g_{5/2} + 6\%d_{5/2} + 46\%d_{3/2} + 7\%s_{1/2}$.

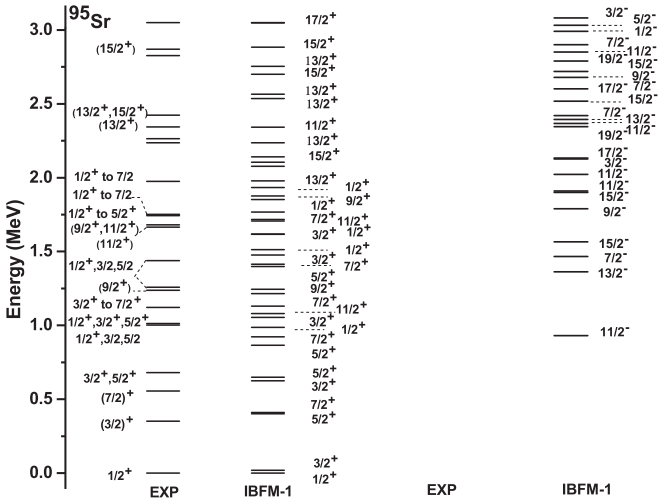

FIG. 5. Same as Fig. 1 but for ^{95}Sr isotope.

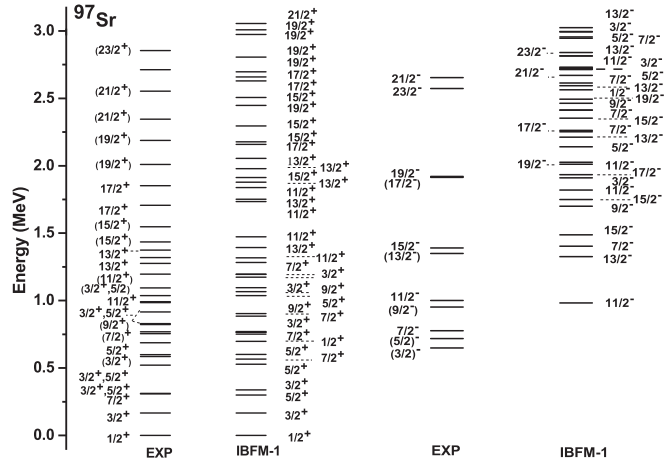

FIG. 6. Same as Fig. 1 but for ^{97}Sr isotope.

The calculated energy of the level $1/2_2^+$ at 0.987 MeV is closed to the experimental level at 1.003 MeV, whereas a $3/2_3^+$ has appeared at 1.012 MeV in agreement with IBFM-1 calculation at 1.055 MeV. The first $9/2^+$ state is somewhat well reproduced. Our calculation has predicted $11/2_2^+$ and $13/2_1^+$ states at 1.718 and 1.980 MeV, respectively. The main components of the wave functions of some states are

$$
\begin{aligned}
|3/2_1^+\rangle &= 47.36\%|0_1^+ \otimes d_{3/2}\rangle + 45.90\%|2_1^+ \otimes g_{7/2}\rangle \\
&\quad + 3.57\%|2_1^+ \otimes d_{5/2}\rangle + \cdots \\
|5/2_1^+\rangle &= 43.64\%|2_1^+ \otimes d_{3/2}\rangle + 36.36\%|2_1^+ \otimes g_{7/2}\rangle \\
&\quad + 14.30\%|2_1^+ \otimes s_{1/2}\rangle + \cdots \\
|7/2_1^+\rangle &= 52.48\%|0_1^+ \otimes g_{7/2}\rangle + 42.80\%|2_1^+ \otimes d_{3/2}\rangle \\
&\quad + 3.04\%|2_1^+ \otimes d_{5/2}\rangle + \cdots \\
|9/2_1^+\rangle &= 39.46\%|3_1^+ \otimes d_{3/2}\rangle + 35.73\%|2_1^+ \otimes g_{7/2}\rangle \\
&\quad + 17.11\%|4_1^+ \otimes s_{1/2}\rangle + \cdots \\
|11/2_1^+\rangle &= 52.32\%|2_1^+ \otimes g_{7/2}\rangle + 43.09\%|4_1^+ \otimes d_{3/2}\rangle \\
&\quad + 3.36\%|3_1^+ \otimes d_{5/2}\rangle + \cdots
\end{aligned}
$$

The calculated spectrum of ^{97}Sr is shown in Fig. 6 together with the experimental data. The main component of the ground state $1/2_1^+$ is the single-quasiparticle state $\upsilon d_{3/2}$ not $\upsilon s_{1/2}$. The first excitation state has $j = 3/2_1^+$ at 0.167 MeV, which is in very good agreement with the IBFM-1 at exactly 0.167 MeV. The wave function of this state is strongly mixed. The structure is $31\%g_{5/2} + 7\%d_{5/2} + 55\%d_{3/2} + 7\%s_{1/2}$. In Ref. [50] the ground state is considered as $3/2^+$ and the first excitation state is $5/2^+$ at 0.167 MeV with 1.5 ns. The low-lying state with 0.312 MeV has not been assigned any other quantum number; it is close to the calculated level at 0.299 MeV with $j = 5/2_1^+$. The first doublets experimental states with uncertain spin assignment $j = 3/2^+, 5/2^+$ at 0.522 and 0.600 MeV have been assigned to the calculated level $5/2_2^+$ and $3/2_3^+$ at 0.528 and 0.752 MeV, respectively. These levels are likely to be spherical [51]. The third experimental $5/2^+$ state at 0.687 MeV agrees very well with IBFM-1 calculation at 0.601 MeV, and its structure is well distributed over the four positive-parity orbitals. The model predicts $1/2_2^+$ and $7/2_2^+$ states at 0.697 and 0.766 MeV, respectively.

In the calculated spectrum, the levels with $j = 7/2_3^+$ and $9/2_1^+$ at 0.885 and 0.771 MeV are in good agreement with the experimental state at 0.822 and 0.831 MeV, respectively. At about 1 MeV there are another two doublets states with the uncertain spin assignment $(3/2^+, 5/2^+)$ at 0.985 and 1.095 MeV. The IBFM reproduced these levels at 1.096 and 1.197 MeV with $j = 3/2_{4,5}^+$, respectively. The calculated energy for the $11/2_{1,2}^+$ and $13/2_1^+$ states at 1.173, 1.317, and 1.394 MeV has been close to the experimental states at 1.036, 1.198, and 1.276 MeV, respectively. Finally, the wave functions of some levels are

$$
\begin{aligned}
|3/2_1^+\rangle &= 54.88\%|0_1^+ \otimes d_{3/2}\rangle + 30.32\%|2_1^+ \otimes g_{7/2}\rangle \\
&\quad + 7.37\%|2_1^+ \otimes d_{5/2}\rangle + \cdots \\
|5/2_1^+\rangle &= 42.85\%|2_1^+ \otimes d_{3/2}\rangle + 29.58\%|2_1^+ \otimes g_{7/2}\rangle \\
&\quad + 17.02\%|2_1^+ \otimes s_{1/2}\rangle + \cdots \\
|7/2_1^+\rangle &= 54.40\%|2_1^+ \otimes d_{3/2}\rangle + 33.51\%|0_1^+ \otimes g_{7/2}\rangle \\
&\quad + 7.38\%|2_1^+ \otimes d_{5/2}\rangle + \cdots \\
|9/2_1^+\rangle &= 39.20\%|3_1^+ \otimes d_{3/2}\rangle + 33.46\%|2_1^+ \otimes g_{7/2}\rangle \\
&\quad + 15.77\%|4_1^+ \otimes s_{1/2}\rangle + \cdots \\
|11/2_1^+\rangle &= 55.01\%|4_1^+ \otimes d_{3/2}\rangle + 32.29\%|2_1^+ \otimes g_{7/2}\rangle \\
&\quad + 9.98\%|2_1^+ \otimes d_{5/2}\rangle + \cdots
\end{aligned}
$$

In the calculation of the negative-parity states in the $^{91-97}$Sr isotopes, we restrict the unpaired neutron to the $h_{11/2}$ orbital. With this choice, the Hamiltonian takes on the same form we discussed in the positive-parity states. The boson-fermion interaction parameters used in these calculations were kept constant as in the positive-parity calculation. With these values, it is found that many calculated levels are quite close to the observed ones. Even if the theoretical states of ^{91,93}Sr isotopes are more densely grouped than the corresponding

TABLE III. Single-particle, quasiparticle energies (in MeV), occupation probabilities and parameters in boson-fermion interaction (in MeV) for $^{91-97}$Y isotopes.

	^{91}Y			^{93}Y			^{95}Y			^{97}Y		
	E	ϵ	υ^2	E	ϵ	υ^2	E	ϵ	υ^2	E	ϵ	υ^2
$1f_{7/2}$	−3.481	3.449	0.986	−3.443	3.412	0.986	−3.407	3.375	0.987	−3.372	3.340	0.987
$1f_{5/2}$	0.489	1.015	0.196	0.469	0.984	0.198	0.451	0.954	0.201	0.433	0.925	0.203
$2p_{3/2}$	0.002	0.816	0.421	0.006	0.795	0.418	0.010	0.775	0.416	0.014	0.756	0.413
$2p_{1/2}$	1.789	2.079	0.039	1.767	2.047	0.038	1.747	2.017	0.037	1.727	1.988	0.036
$1g_{9/2}$	2.849	3.084	0.017	2.839	3.065	0.016	2.829	3.046	0.015	2.819	3.029	0.015
Γ		1.150			1.090			1.090			1.090	
Λ		0.020			0.020			0.020			0.020	
A_0		−0.005			−0.005			−0.005			−0.005	

observed ones. In Figs. 3–6, the calculated results have been shown. The corresponding $11/2^-$ state becomes the lowest state in $^{91-97}$Sr isotopes. For ^{91}Sr, the $11/2^-$ state observed at 2.077 MeV, which arises from the multiplet based on the 0_1^+ state in the core nucleus. A pronounced diagram of the ^{95}Sr isotope experimental data is that no negative-parity states were observed below 3 MeV. The calculated $11/2_1^-$ state at 0.953 MeV, while the second excited state $J^\pi = 13/2^-$ appears at 1.382 MeV. For ^{97}Sr isotope, the negative parity states are shown in Fig. 6. The low-lying unfavored J^- states, of uncertainly spin $(3/2)^-$ (0.644 MeV) and $(5/2)^-$ (0.713 MeV) exhibit disagreement, which cannot be fitted by the calculation. The calculated $7/2_1^-$ state at 0.895 MeV is close to the experimental one at 0.771 MeV, while the model calculation gives the $9/2_1^-$ state at 1.193 MeV and it is far from the experimental $(9/2_1^-)$ at 0.946 MeV.

C. Odd-proton $^{91-97}$Y nuclear structure

For Yttrium isotopes, we have considered the energy levels structure of the $^{91-97}$Y as the result of a proton quasiparticle coupled to the $^{90-96}$Sr even-even cores, respectively. The BCS equations were solved with the single-particle orbitals $1f_{7/2}$, $1f_{5/2}$, $2p_{3/2}$, $2p_{1/2}$, and $1g_{9/2}$. The single-particle energies are extracted from Ref. [48]. The quasiparticle energies and occupation probabilities are listed in Table III. The $f_{7/2}$ orbital is the most probable to be occupied by a fermion ($\upsilon^2 \approx 0.98$) and the probability increases with increasing the mass number of the nuclei. The coupling of a $g_{9/2}$ quasiparticle to the harmonic U(5) boson core is studied by Scholten in an interpretative IBFM model [52]. The value of $\Lambda = 0.020$ and $A_0 = -0.005$ MeV have been used for all isotopes. Other parameters do not differ too much among neighboring nuclei. The strength of the quadrupole force Γ in the $V_{\rm BF}$ has to be decreased to lower the energy of the first $3/2^-$ state in ^{93}Y nucleus. A comparison of the results of IBFM-1 calculations with the experimental results [43] on the low-lying negative-parity states of $^{91-97}$Y isotopes is shown in Figs. 7–10.

One can see from Fig. 7 that the calculated energy of the $7/2_1^-$ and $3/2_2^-$ levels agree very well with the experimental data in ^{91}Y isotope. The state with uncertain spin assignment $7/2_2^-, 9/2_1^-$ is at an excitation energy of 1.547 MeV. It has been reproduced well in the IBFM-1 calculation with excitation energy of 1.856 MeV ($j = 7/2_2^-$). It has a configuration of $37\%p_{3/2} + 27\%f_{5/2} + 26\%p_{1/2} + 10\%f_{7/2}$. The third $j = 5/2^-$ state at energy 2.071 MeV is close to the experimental state at 1.980 MeV, and the wave function of this level is strongly mixed. The structure is $38\%f_{5/2} + 34\%p_{3/2} + 22\%p_{1/2} + 6\%f_{7/2}$. The wave functions of some states are

$$
\begin{aligned}
|1/2_1^-\rangle &= 41.33\%|2_1^+ \otimes f_{5/2}\rangle + 36.72\%|0_1^+ \otimes p_{1/2}\rangle \\
&\quad + 19.65\%|2_1^+ \otimes p_{3/2}\rangle + \cdots \\
|3/2_1^-\rangle &= 32.18\%|0_1^+ \otimes p_{3/2}\rangle + 30.82\%|2_1^+ \otimes f_{5/2}\rangle \\
&\quad + 31.84\%|2_1^+ \otimes p_{1/2}\rangle + \cdots \\
|5/2_1^-\rangle &= 54.60\%|0_1^+ \otimes f_{5/2}\rangle + 31.25\%|2_1^+ \otimes p_{1/2}\rangle \\
&\quad + 12.95\%|2_1^+ \otimes p_{3/2}\rangle + \cdots \\
|7/2_1^-\rangle &= 36.67\%|2_1^+ \otimes p_{3/2}\rangle + 27.05\%|2_1^+ \otimes f_{5/2}\rangle \\
&\quad + 26.53\%|3_1^+ \otimes p_{1/2}\rangle + \cdots \\
|9/2_1^-\rangle &= 58.75\%|2_1^+ \otimes f_{5/2}\rangle + 29.92\%|4_1^+ \otimes p_{1/2}\rangle \\
&\quad + 10.51\%|3_1^+ \otimes p_{3/2}\rangle + \cdots
\end{aligned}
$$

In ^{93}Y as shown in Fig. 8, the energy levels $j = 3/2_1^-, 5/2_1^-$ is higher than the ones in the previous nucleus. The model approaches somewhat close to computing the energy of level $3/2_1^-$ while failing to calculate the other

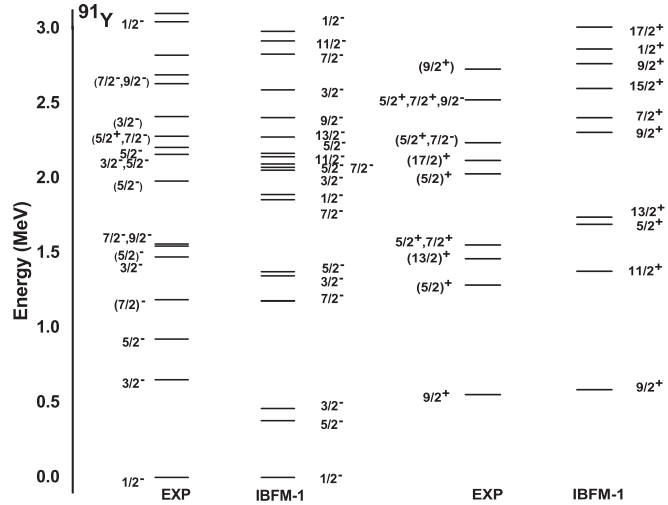

FIG. 7. Same as Fig. 1 but for ^{91}Y isotope.

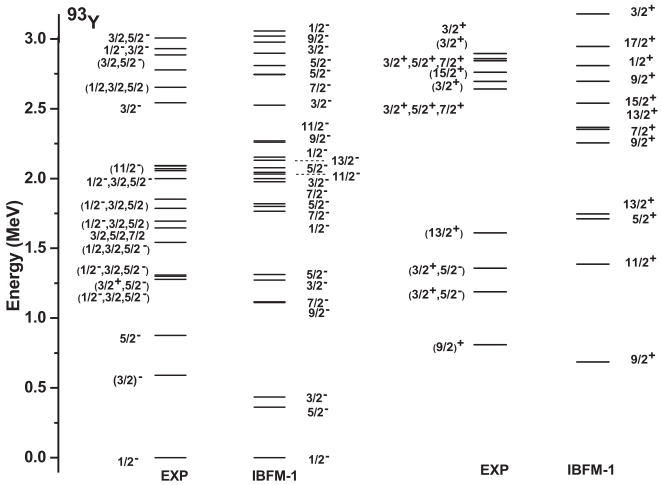

FIG. 8. Same as Fig. 1 but for ^{93}Y isotope.

energy level. Experimentally, the level at 1.278 MeV has possible $j = (1/2^-, 3/2, 5/2^-)$ assignment close to 1.272 MeV with $j = 3/2_2^-$ in the IBFM-1 calculation. Another state at 1.300 MeV has possible $j = (3/2^+, 5/2^-)$ assignment close to 1.311 MeV with $j = 5/2_2^-$ in experimental data and IBFM-1 results, respectively. The wave functions of some levels are

$$|1/2_1^-\rangle = 41.31\%|2_1^+ \otimes f_{5/2}\rangle + 36.46\%|0_1^+ \otimes p_{1/2}\rangle + 19.76\%|2_1^+ \otimes p_{3/2}\rangle + \cdots$$

$$|3/2_1^-\rangle = 32.66\%|2_1^+ \otimes p_{1/2}\rangle + 32.42\%|2_1^+ \otimes f_{5/2}\rangle + 30.04\%|0_1^+ \otimes p_{3/2}\rangle + \cdots$$

$$|5/2_1^-\rangle = 52.57\%|0_1^+ \otimes f_{5/2}\rangle + 32.18\%|2_1^+ \otimes p_{1/2}\rangle + 13.87\%|2_1^+ \otimes p_{3/2}\rangle + \cdots$$

$$|7/2_1^-\rangle = 33.92\%|2_1^+ \otimes p_{3/2}\rangle + 29.11\%|2_1^+ \otimes f_{5/2}\rangle + 28.42\%|3_1^+ \otimes p_{1/2}\rangle + \cdots$$

$$|9/2_1^-\rangle = 56.33\%|2_1^+ \otimes f_{5/2}\rangle + 31.08\%|4_1^+ \otimes p_{1/2}\rangle + 11.58\%|3_1^+ \otimes p_{3/2}\rangle + \cdots$$

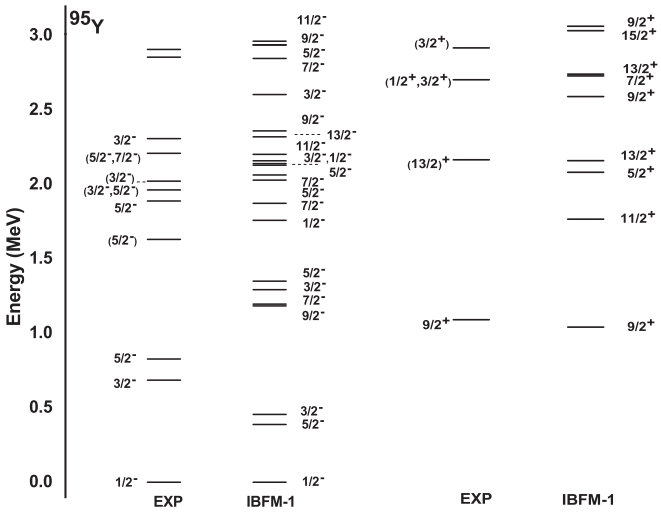

FIG. 9. Same as Fig. 1 but for ^{95}Y isotope.

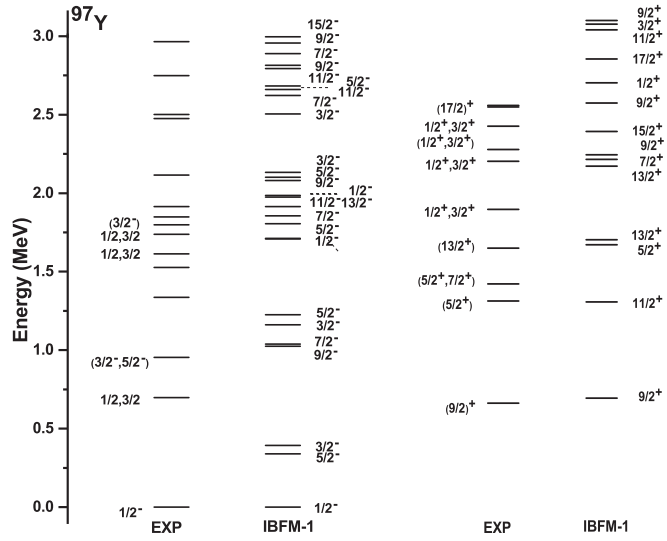

FIG. 10. Same as Fig. 1 but for ^{97}Y isotope.

Figure 9 presents a more detailed comparison between experimental and calculated energy states in ^{95}Y isotope. It is worth noticing that the IBFM-1 calculations have been based on the same interaction parameters of ^{93}Y isotope, and the agreement with the available experimental data appears to be good. The ground state is $1/2^-$.The observed levels $5/2_2^-$ and $5/2_3^-$ at (1.630 and 1.889) MeV are in agreement with IBFM-1 calculations at (1.351 and 2.029), respectively. The model predicted the appearance of $13/2_1^-$ state at 2.321. The percentages of the main components in the wave functions of the lowest levels are

$$|1/2_1^-\rangle = 40.99\%|2_1^+ \otimes f_{5/2}\rangle + 36.76\%|0_1^+ \otimes p_{1/2}\rangle + 19.66\%|2_1^+ \otimes p_{3/2}\rangle + \cdots$$

$$|3/2_1^-\rangle = 33.36\%|2_1^+ \otimes p_{1/2}\rangle + 32.47\%|4_1^+ \otimes f_{5/2}\rangle + 29.14\%|0_1^+ \otimes p_{3/2}\rangle + \cdots$$

$$|5/2_1^-\rangle = 51.18\%|0_1^+ \otimes f_{5/2}\rangle + 33.14\%|2_1^+ \otimes p_{1/2}\rangle + 14.18\%|2_1^+ \otimes p_{3/2}\rangle + \cdots$$

$$|7/2_1^-\rangle = 33.36\%|2_1^+ \otimes p_{3/2}\rangle + 29.03\%|3_1^+ \otimes p_{1/2}\rangle + 28.51\%|2_1^+ \otimes f_{5/2}\rangle + \cdots$$

$$|9/2_1^-\rangle = 55.22\%|2_1^+ \otimes f_{5/2}\rangle + 31.94\%|4_1^+ \otimes p_{1/2}\rangle + 11.75\%|3_1^+ \otimes p_{3/2}\rangle + \cdots$$

The calculated spectrum of ^{97}Y isotope has been shown in Fig. 10 together with the experimental data. It is interesting to note that the IBFM-1 calculations reproduce the available experimental data well. The $5/2_1^-$ state calculated at 0.339 MeV is not observed experimentally. The calculated wave function is $2\%f_{7/2} + 49\%f_{5/2} + 15\%p_{3/2} + 34\%p_{1/2}$. The second excitation state with uncertain $(1/2, 3/2)$ assignment at 0.697 MeV is somewhat close to the $3/2^-$ state within an error of about 300 KeV. The wave functions of some states

are

$$
\begin{aligned}
|1/2_1^-\rangle &= 41.14\%|2_1^+ \otimes f_{5/2}\rangle + 36.16\%|0_1^+ \otimes p_{1/2}\rangle \\
&\quad + 19.84\%|2_1^+ \otimes p_{3/2}\rangle + \cdots \\
|3/2_1^-\rangle &= 35.04\%|2_1^+ \otimes f_{5/2}\rangle + 34.04\%|2_1^+ \otimes p_{1/2}\rangle \\
&\quad + 26.36\%|0_1^+ \otimes p_{3/2}\rangle + \cdots \\
|5/2_1^-\rangle &= 48.63\%|0_1^+ \otimes f_{5/2}\rangle + 33.94\%|2_1^+ \otimes p_{1/2}\rangle \\
&\quad + 15.60\%|2_1^+ \otimes p_{3/2}\rangle + \cdots \\
|7/2_1^-\rangle &= 32.22\%|2_1^+ \otimes f_{5/2}\rangle + 31.42\%|2_1^+ \otimes p_{1/2}\rangle \\
&\quad + 29.35\%|2_1^+ \otimes p_{3/2}\rangle + \cdots \\
|9/2_1^-\rangle &= 51.83\%|2_1^+ \otimes f_{5/2}\rangle + 33.19\%|4_1^+ \otimes p_{1/2}\rangle \\
&\quad + 13.57\%|3_1^+ \otimes p_{3/2}\rangle + \cdots \\
|11/2_1^-\rangle &= 32.66\%|4_1^+ \otimes p_{3/2}\rangle + 28.34\%|5_1^+ \otimes p_{1/2}\rangle \\
&\quad + 28.13\%|3_1^+ \otimes f_{5/2}\rangle + \cdots
\end{aligned}
$$

The $^{91-97}$Y positive parity states have been calculated in the one single-particle orbital ($g_{9/2}$). For the interaction parameters we have started with the values of negative states calculation, looking for a better description of the spectra, as discussed in the following. The assignments of the theoretical states to experimental ones are made by considering several observables. We have finally used the same for both parities. Although modest adjustments to their values would get better the fit to the energies, we opted to leave them alone. It is difficult to produce positive parity levels by keeping the same value of the single-particle energy of $g_{9/2}$ orbit, particularly the first $9/2^+$ state. This difficulty was pointed out in IBFM calculations [53–55]. The fitting improves only if the relative energy of $g_{9/2}$ orbit is changed. The quasiparticle energy of the ($g_{9/2}$) has been decreased to obtain the energy of the first excited $J^\pi = 9/2^+$. A comparison of the model results and experimental data is shown in Figs. 7–10. However, in $^{91-97}$Y isotopes a $9/2^+$ state has been observed at 0.555, 0.758, 1.087, and 0.667 MeV as a lowest positive-parity state, respectively

Although we have obtained a good satisfactory description for the spectrum, one could have doubts of the other single-particle orbital ($d_{5/2}$) from the next major shell. In ^{91}Y isotope, experimentally the state at 1.579 MeV has possible $J^\pi = 5/2^+7/2^+$. It is close to a state at 1.650 MeV with $J = 5/2^+$ in our model calculation. The first calculated $J = 13/2^+$ state at 1.689 MeV is close to experimental one at 1.485 MeV. The calculated results show that $J = 1/2^+$ appears at 2.778 MeV and there is no $J = 3/2^+$ below 3 MeV.

The IBFM energy levels and available experimental data of ^{93}Y isotope are compared in Fig. 8. The calculated $13/2^+$ at 1.684 MeV close to the excitation 1.550 MeV ($13/2^+$). Our model calculation for the $J = 3/2^+$ state is at 3.115 1MeV a little overrated. In the ^{95}Y isotope, the first calculated $5/2^+$ appears at 2.088 MeV and the experimental data up to 3 MeV is scarce. On the other hand, the calculated $J = 13/2_1^+$ state at 2.167 MeV is close to experimental one $(13/2)^+$ at 2.173 MeV.

By including all experimental states up to 3 MeV, the comparison with the theoretical results in ^{97}Y exhibits a good position for many states as shown in Fig. 10. The $(9/2)^+$ at 0.667 MeV is the lowest negative-parity state. The model predicted $11/2^+$ state at 1.313 MeV has not been observed. In the calculation, there is not a $J^+ = 1/2^+$ below 2.5 MeV. Experimentally, there are four $J^+ = 1/2^+, 3/2^+$ states. There is no suitable solution in our model space for this disagreement.

TABLE IV. The model configurations for the proton and neutron used for the description of the $^{92-98}$Y nuclei.

$^{92-98}$Y	$^{91-97}$Sr	$^{91-97}$Y
$\pi = -$	$g_{7/2}, d_{5/2}, d_{3/2}, s_{1/2}$	$f_{7/2}, f_{5/2}, p_{3/2}, p_{1/2}$
	$h_{11/2}$	$g_{9/2}$
$\pi = +$	$g_{7/2}, d_{5/2}, d_{3/2}, s_{1/2}$	$g_{9/2}$
	$h_{11/2}$	$f_{7/2}, f_{5/2}, p_{3/2}, p_{1/2}$

D. Odd-odd $^{92-98}$Y nuclear structure

To calculate the positive- and negative-parity states, the model Hamiltonian was diagonalized with the configurations for the proton and neutron as shown in Table IV. The energy levels of these nuclei were often experimentally uncertain. However, we tried to reach satisfactory results that simulate the observed energy spectrum. We now focus on the discussion of the low-lying states with the IBFFM-1 results as shown in Figs. 11–14. We have searched the ideal values of the residual interaction parameters to reasonably reproduce the low-lying spectra in odd-odd nuclei to get an overall agreement with the experimental properties. The strength parameters of the V_{res} interaction (in MeV)are: $V_{\sigma\sigma} = 0.024$, 0.074, 0.014, and 0.014 while the $V_s = -0.045$, -0.088, -0.122, and -0.045 for $^{92-98}$Y isotopes, respectively.

The negative parity states of the ^{92}Y isotope are shown been offered in Fig. 11. The results of $J^- = \pi(g_{7/2}, d_{5/2}, d_{3/2}, s_{1/2})\nu(f_{7/2}, f_{5/2}, p_{3/2}, p_{1/2})$ calculation can be viewed as below. The ground state with certain spin assignment is $J^\pi = 2^-$ in the experimental [43] and IBFFM-1, in which the strongest component is $(\upsilon d_{5/2} \otimes \pi f_{5/2})$. The main components of the wave functions of low-lying states are presented in Table V. According to the IBFFM-1 results, the first excited 3_1^- state is at 0.061 MeV, while experimentally, the angular momentum value of the first excited state was not determined. The experimental states with uncertain spin assignment $J^\pi = (0^-, 2, 3^+)$ at 0.242 MeV were assigned to the calculated 0_2^- state at 0.177 MeV. Another experimental state with uncertain spin assignment $J^\pi = (2^-, 3^-, 4^-)$ at 0.310 MeV was assigned to the calculated 2_2^- state at 0.259 MeV. The calculated 2_3^- state at 0.560 MeV was close to the uncertain spin assignment $J^- = (2)^-$ with experimental energy at 0.430 MeV. The major component in the wave functions of the lowest three negative-parity states, i.e., 3_1^-, 1_1^-, and 0_1^- states, is the $(\upsilon d_{5/2} \otimes \pi f_{5/2})$ neutron-proton pair. The $(\upsilon g_{7/2} \otimes \pi f_{5/2})$ component is a dominating component in the levels 4_1^-, 6_1^-, 8_1^-, and 10_1^- states. The $(\upsilon d_{5/2} \otimes \pi f_{5/2})$ component is strong in the levels 5_1^-, 7_1^-, and 9_1^- states. We used the same model parametrization to describe the negative-parity states based on the $\nu h_{11/2}\pi g_{9/2}$ (2-qp state). In this

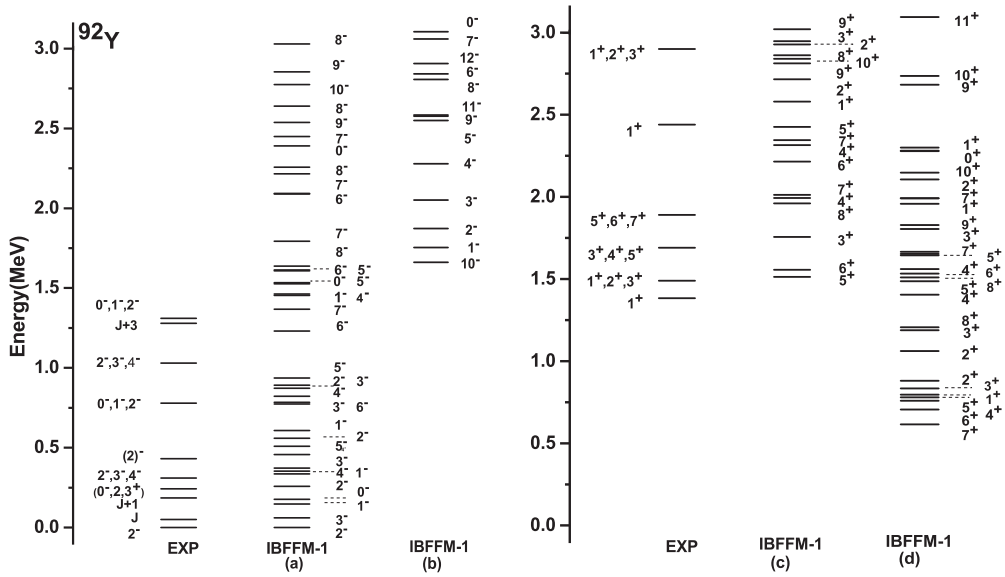

FIG. 11. Calculated and observed energy spectra [43] for ^{92}Y isotope. (a) and (b) IBFFM negative energy spectrum levels of the $[\nu(g_{7/2}d_{5/2}d_{3/2}s_{1/2})\pi(f_{7/2}f_{5/2}p_{3/2}p_{1/2})]$ and $[\nu h_{11/2}\pi g_{9/2}]$ configuration, while (c) and (d) IBFFM positive energy levels of the $[\nu(h_{11/2})\pi(f_{7/2}f_{5/2}p_{3/2}p_{1/2})]$ and $[\nu(g_{7/2}d_{5/2}d_{3/2}s_{1/2})\pi g_{9/2})]$ configuration, respectively.

calculation, the lowest state appears at 1.664 MeV ($J^\pi = 10^-$).

Calculated positive parity states are shown in Fig. 11 columns c and d, which are based on the $[\nu(h_{11/2})\pi(f_{7/2}f_{5/2}p_{3/2}p_{1/2})]$ and $[\nu(g_{7/2}d_{5/2}d_{3/2}s_{1/2})\pi g_{9/2})]$ configurations, respectively. The wave function of the first appear of the states $J^\pi = 1^+$–8^+ comes from $[\nu(h_{11/2})\pi(f_{5/2}p_{1/2})]$. The 3^+ state component in the model calculation amounts to $[100\%h_{11/2} \otimes (59\%f_{5/2} + 27\%p_{1/2})]$. While the 1^- state arising from the $[100\%h_{11/2} \otimes (64\%f_{5/2} + 26\%p_{1/2})]$. This level is tentatively assigned to the experimental 1^+ at 2.440 MeV. For the positive-parity levels, a structure based on the $\pi g_{9/2}$ configuration is predicted. The low-lying members $J^+ = 2^+ - 7^+$ mainly have a common configuration of $\nu(d_{5/2})$. The calculation also reproduces the 1^+_1 state with $100\%\pi g_{9/2} \otimes 91\%\nu d_{5/2}$.

The comparison of energy levels of the odd-odd ^{94}Y nucleus is shown in Fig. 12, one can conclude that the calculations are able to reproduce the experimental negative parity states reasonably. The first excited negative state $J = 3^-_1$ arising from $\%92d_{5/2} \otimes (42\%f_{5/2} + 18\%p_{3/2} + 36\%p_{1/2})$ assigned to the 0.435 MeV [43].

The structure of the 0^-_1, and 1^-_1 states is dominated by the $(\upsilon d_{5/2} \otimes \pi f_{5/2})_{J=0^-_1,1^-_1}$ pair component. The IBFFM calculations show that the 2^-_2 has the $(91\%\upsilon d_{5/2} \otimes 48\%\pi f_{5/2})$ as a main configuration. The main components of the wave func-

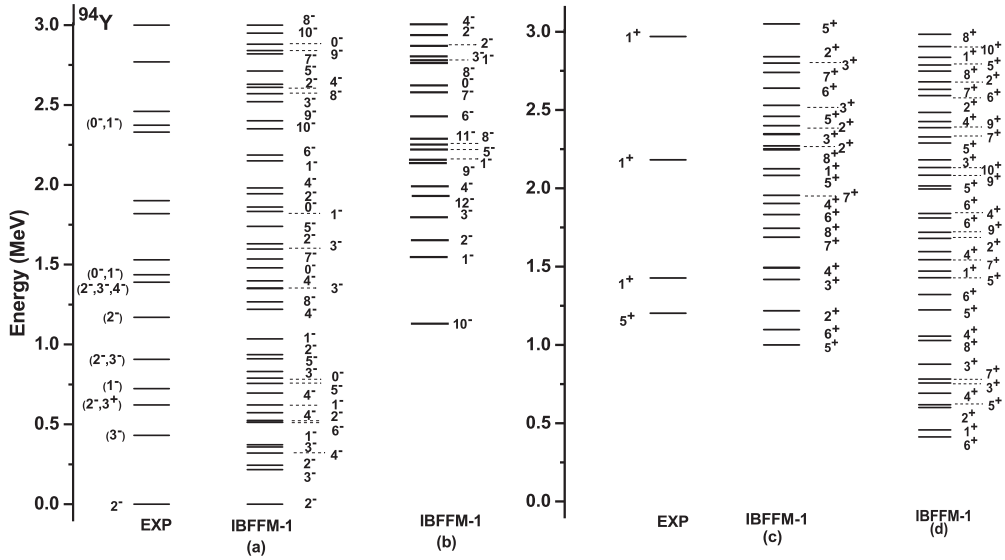

FIG. 12. Same as Fig. 11 but for ^{94}Y isotope.

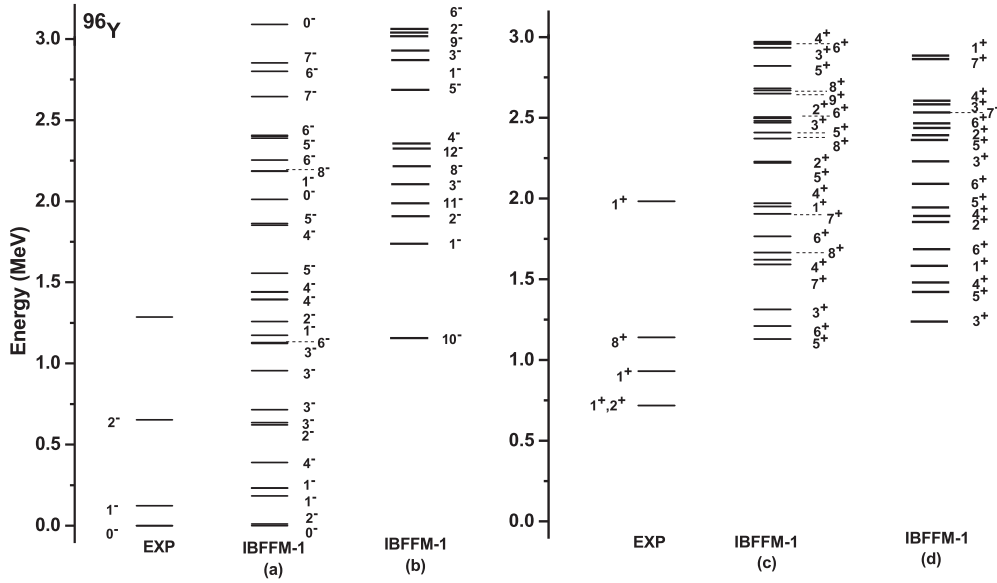

FIG. 13. Same as Fig. 11 but for ^{96}Y isotope.

tions of low-lying states are listed in Table V. Experimentally, there are three $J^+ = 1^+$ states at 1.427, 2.182, 2.969 MeV. These levels arise from the configurations in columns c and d.

For ^{96}Y isotope, the IBFFM results have been compared with available experimental states in Fig. 13. The first level $J^\pi = 1^-$ with excitation energy at 0.183 MeV in agreement with the experimental data at 0.122 MeV. The other level is $J^\pi = 2^-_2$ at 0.622 MeV and 0.652 MeV in IBFFM-1 and experimental data, respectively. The strength of the $(\upsilon d_{3/2} \otimes \pi f_{5/2})$ configuration in the wave function is more than 88% for the levels 1^-_1 and 2^-_1. The pronounced experimental spectrum of ^{96}Y shows that there are no low-energy states in the interval between 1^-_1 and 2^-_1 states. In our calculations, this gap has four levels. The calculated energy levels closely matched those from Ref. [56]. The IBFFM results show that the 4^-_1 and 3^-_1 have the main configuration $(\upsilon g_{7/2} \otimes \pi f_{5/2})$, and the 4^-_1 state lying below the 5^-_1 state. The main components of the wave functions of low-lying states are presented in Table VI. Using the $(\upsilon h_{11/2} \otimes \pi g)_{9/2}$, the negative-parity state has been calculated. We obtain $J^\pi = 10^-$ as the lowest state at 1.156 MeV. The lowest-lying 3^+ level belong to $\nu g_{7/2} \pi g_{9/2}$ multiplet, and it is separated from the 3^+ level member of the to $\nu h_{11/2} \pi f_{5/2}$ multiplet. It can be seen that the 1^+, 2^+ (0.718 MeV) and 1^+ (0.931 MeV) observed states can not be assigned to model calculation. These states could be intruder states generated from the 0^+ intruder state in the ^{94}Sr core. The lowest 1^+_1 state come from $\nu g_{7/2} \pi g_{9/2}$ quasiparticles at 1.623 MeV. The 1^+_2 state at energy 0.1.951 MeV is close to the experimental level at 1.983 MeV with $\nu h_{11/2} \pi f_{5/2}$ configuration.

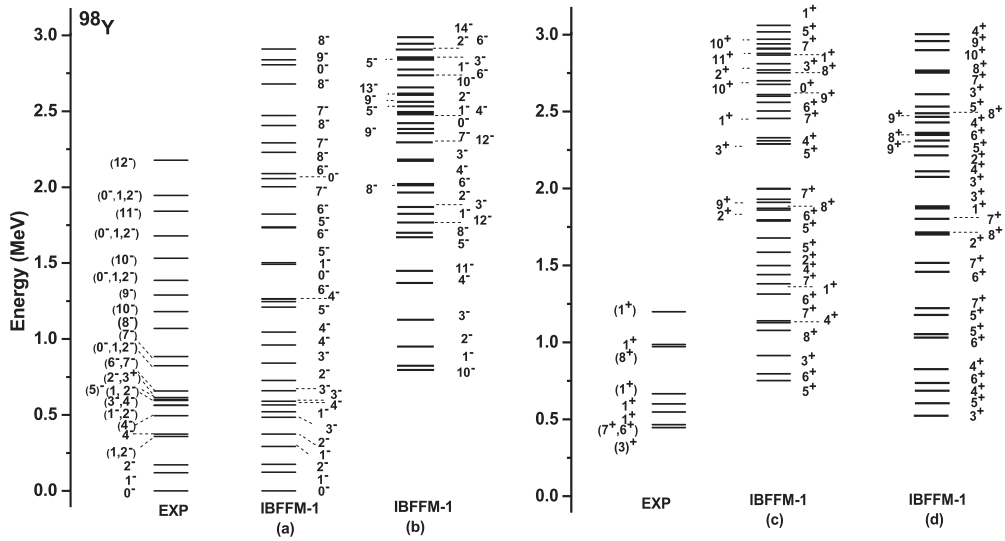

FIG. 14. Same as Fig. 11 but for ^{98}Y isotope.

TABLE V. The percentage components of wave functions, some of available experimental and calculated energy stats for ^{92,94}Y.

IBFFM-1						^{92}Y				EXP	
J^-	Energy	$\upsilon g_{7/2}$	$\upsilon d_{5/2}$	$\upsilon d_{3/2}$	$\upsilon s_{1/2}$	$\pi f_{7/2}$	$\pi f_{5/2}$	$\pi p_{3/2}$	$\pi p_{1/2}$	J^-	Energy
2_1^-	0.000	3.48	86.92	2.84	6.76	2.53	39.56	21.68	36.23	2^-	0.000
3_1^-	0.061	3.44	86.96	3.00	6.87	1.93	42.81	19.02	36.24	J	0.0+x
0_2^-	0.177	38.53	38.44	17.04	5.99	5.35	35.04	40.77	18.84	$(0^-, 2, 3^+)$	0.242
2_2^-	0.259	24.34	58.21	12.99	4.46	1.88	47.07	18.50	32.54	$2^-, 3^-, 4^-$	0.310
2_3^-	0.560	35.89	43.69	15.33	5.09	2.01	47.26	18.44	32.29	$(2)^-$	0.430
2_4^-	0.872	2.74	90.91	1.03	5.31	5.31	32.18	32.64	29.87	$0^-, 1^-, 2^-$	0.780
IBFFM-1						^{94}Y				EXP	
2_1^-	0.000	3.89	91.92	0.43	3.76	2.81	35.72	23.95	37.53	2^-	0.000
3_1^-	0.237	4.15	92.52	0.52	2.81	1.95	42.53	18.75	36.78	(3^-)	0.432
2_3^-	0.527	72.74	7.15	19.55	0.56	3.18	38.40	26.37	32.05	$(2, 3^+)$	0.622
2_4^-	0.936	8.24	88.81	0.50	2.44	4.63	32.60	31.81	30.95	$(2^-, 3^-)$	0.907
2_5^-	1.331	22.16	72.65	2.29	2.91	4.75	46.71	22.30	26.25	(2^-)	1.170
3_4^-	1.303	8.08	88.43	0.64	2.85	3.26	46.53	22.14	28.07	$(2^-, 3^-, 4^-)$	1.390

The calculated spectrum of the negative and positive-parity states in ^{98}Y has been displayed in Fig. 14. The ground state and the low-lying levels in our calculations are correctly reproduced. The IBFFM calculation confirms these results, where the 0_1^- ground state has the dominating configuration $(\upsilon d_{3/2} \otimes \pi f_{5/2})$. Experimentally, the 1_1^- and 2_1^- states have been assigned to the 0.119 and 0.171 MeV, respectively. while the model energies are equal to 0.123 MeV and 0.174 MeV, respectively. Furthermore, these calculated states are based on the $(\upsilon d_{3/2} \otimes \pi f_{5/2})$ configuration. The spherical level at 0.375 MeV has been reported as J = 2^- [57], and this is exactly in agreement with our calculation at 0.375 MeV with J = 2_2^-. On one hand, it is assigned as a probable 4^- state as in Table 2 in Ref. [58]. The calculated level 4_1^- at 0.590 MeV is close to J = $(4)^-$ at 0.496 MeV, and based on the $(\upsilon d_{3/2} \otimes \pi f_{5/2})$ configuration with sizeable admixtures of $(\upsilon g_{7/2} \otimes \pi p_{1/2})$ components. The 1_2^- and 2_2^- states have been based on the $\upsilon d_{3/2} \otimes \pi f_{5/2}$ and $\upsilon d_{3/2} \otimes \pi p_{1/2}$ configuration. However, our calculations fail to reproduce the position of the 8_1^-, and 7_1^- states. The level with uncertain J = $(1^-, 2^-)$ is

TABLE VI. The percentage components of wave functions, some of available experimental and calculated energy stats for ^{96,98}Y.

IBFFM-1						^{96}Y				EXP	
J^-	Energy	$\upsilon g_{7/2}$	$\upsilon d_{5/2}$	$\upsilon d_{3/2}$	$\upsilon s_{1/2}$	$\pi f_{7/2}$	$\pi f_{5/2}$	$\pi p_{3/2}$	$\pi p_{1/2}$	J^-	Energy
0_1^-	0.000	38.10	4.98	46.98	9.49	3.58	38.09	24.39	33.94	0^-	0.000
1_1^-	0.184	40.09	4.90	47.20	7.81	3.01	40.93	22.09	33.97	1^-	0.122
2_2^-	0.622	43.33	4.74	47.30	4.62	5.15	32.98	29.48	32.39	2^-	0.652
3_1^-	0.635	49.44	4.20	43.24	3.12	3.51	35.57	26.79	34.14		
3_2^-	0.715	38.59	5.81	43.58	11.67	1.44	49.36	15.59	33.61		
2_3^-	0.956	39.20	13.16	38.60	9.04	5.55	35.76	24.97	33.73		
2_4^-	0.956	40.39	13.17	37.76	8.68	2.97	39.15	21.38	36.50		
IBFFM-1						^{94}Y				EXP	
0_1^-	0.000	28.40	8.91	48.82	13.88	4.53	37.18	23.16	35.12	0^-	0.000
1_1^-	0.123	28.83	9.40	49.00	12.77	3.62	40.64	20.45	35.30	1^-	0.119
2_1^-	0.175	30.91	8.07	52.91	8.11	3.28	43.25	19.06	34.41	2^-	0.171
1_2^-	0.293	32.18	7.76	52.20	7.86	4.42	36.96	23.66	34.96	$(1, 2^-)$	0.358
2_2^-	0.375	30.19	20.69	35.97	13.32	6.57	33.94	25.37	34.12	4^-	0.375
4_2^-	0.590	33.43	7.74	52.65	6.19	2.36	47.10	16.39	34.16	$(4)^-$	0.496
1_3^-	0.566	40.84	10.33	44.10	4.73	6.45	34.02	24.86	34.68	$(1^-, 2^-)$	0.564
3_1^-	0.590	28.86	21.48	35.89	13.76	3.24	42.26	18.83	35.67	$(3^-, 4^-)$	0.564+x
2_3^-	0.485	39.54	11.76	43.00	5.70	4.80	40.12	20.89	34.19	$(1, 2^-)$	0.596

TABLE VII. A comparison between IBM-1 and experimental data of $B(E2)$ values in e^2b^2 unit for $^{90-96}$Sr isotopes. The available experimental data is given in the second row.

$I_i^+ \to I_f^+$	^{90}Sr IBM-1	^{92}Sr IBM-1	^{94}Sr IBM-1	^{96}Sr IBM-1
$2_1^+ \to 0_1^+$	0.0183	0.0214	0.0249	0.0282
		0.0197(73)	0.0203(101)	0.0339(209)
$4_1^+ \to 2_1^+$	0.0304	0.0366	0.0434	0.0499
$6_1^+ \to 4_1^+$	0.0365	0.0456	0.0556	0.0652
$8_1^+ \to 6_1^+$	0.0364	0.0486	0.0615	0.0742
$0_2^+ \to 2_1^+$	0.0302	0.0363	0.0425	0.0488
				0.0399(4)
$0_2^+ \to 2_2^+$	0.0000	0.0000	0.0000	0.0000
$0_3^+ \to 2_1^+$	0.0000	0.0000	0.0000	0.0000
		0.0006		0.0001
$2_2^+ \to 0_1^+$	0.0000	0.0000	0.0000	0.0000
		0.0009(4)		
$2_2^+ \to 2_1^+$	0.0304	0.0366	0.0434	0.0499
				>0.0232
$2_3^+ \to 0_1^+$	0.0000	0.0000	0.0000	0.0000
$2_3^+ \to 2_1^+$	0.0000	0.0000	0.0000	0.0000
		⩾0.003		0.0000
$4_2^+ \to 2_1^+$	0.0000	0.0000	0.0000	0.0000
$4_2^+ \to 2_2^+$	0.0191	0.0239	0.0291	0.0342
$4_2^+ \to 4_1^+$	0.0174	0.0217	0.0265	0.0311

close to our calculations at 0.566 MeV with J = 1_3^- [58]. The main components of the wave functions of low-lying states are presented in Table VI.

E. Electromagnetic transition

We can calculate the electromagnetic transition probabilities of the energy levels using the model wave function. In IBM-1 the $E2$ operator is expressed as [37]:

$$\hat{T}_B(E2) = \alpha_2[d^\dagger \times s + s^\dagger \times \tilde{d}]^{(2)} + \beta_2[d^\dagger \times \tilde{d}]^{(2)}. \quad (17)$$

The electromagnetic transition operator in the IBFM-1 is written as follows:

$$\hat{T} = \hat{T}_B + \hat{T}_F. \quad (18)$$

The first term is concerned only with the part related to the boson, and the second deals with the fermion. The $(E2)$ transition operator can be written as:

$$\hat{T}^{E2} = \hat{T}_B(E2) + e_F \sum_{jj'} Q_{jj'}(a_j^\dagger \times \tilde{a}_{j'})^{(2)}, \quad (19)$$

where e_F is the fermion effective charge and $Q_{jj'}$ is single-particle quadruple operator for fermion. The fermion effective charge is related to the shell model effective charge e^{ff} by:

$$e_F = -\sqrt{1/5}e^{ff}\langle nl|r^2|n'l'\rangle\langle l\,j \parallel Y^{(2)} \parallel l'\,j'\rangle, \quad (20)$$

where the matrix elements are evaluated by the harmonic oscillator wave function. The $M1$ transition operator in IBFM-1 is

$$T^{(M1)} = \sqrt{\frac{30}{4\Pi}}g_b(d^\dagger \times \tilde{d})^{(1)} - \sum_{jj'} g_{jj'}\sqrt{\frac{j(j+1)(2j+1)}{4\pi}}(a_j^\dagger \times \tilde{a})^{(1)}, \quad (21)$$

where g_b is the g factor determined by the even-even core, $g_{jj'}$ is the contribution of single nucleon, which depends on g_ℓ(orbital) and g_s(spin) factors.

TABLE VIII. Calculated $B(E2)$ values (in unit e^2b^2) and $B(M1)$ values (in unit μ_N^2) for $^{91-97}$Sr isotopes. The available experimental data is given in the second row.

$j_i^+ \to j_f^+$	^{91}Sr $B(E2)$	^{91}Sr $B(M1)$	^{93}Sr $B(E2)$	^{93}Sr $B(M1)$	^{95}Sr $B(E2)$	^{95}Sr $B(M1)$	^{97}Sr $B(E2)$	^{97}Sr $B(M1)$
$7/2_1 \to 5/2_1$	0.0002	0.0009	0.0040	0.0017			0.0014	0.0339
$7/2_2 \to 3/2_1$							0.0063	
							0.0047(26)	
$7/2_2 \to 5/2_1$	0.0136	0.0202	0.0312	0.0248	0.0002	0.0009	0.0055	0.1307
$3/2_2 \to 3/2_1$	0.0042	0.0001	0.0041	0.0006	0.0231	0.0182	0.0520	0.0001
$5/2_3 \to 3/2_2$					0.0233	0.0042	0.0145	0.0122
								0.0137(197)
$5/2_2 \to 5/2_1$	0.0287	0.0070	0.0053	0.0211	0.0146	0.0131	0.0126	0.0737
$3/2_2 \to 5/2_1$	0.0020	0.0045	0.0000	0.0021	0.0100	0.0037	0.0318	0.0082
$3/2_1 \to 1/2_1$	0.0214	0.6146			0.0246	0.1105	0.0429	0.0337
								0.0376(71)
$7/2_2 \to 7/2_1$	0.0001	0.0107	0.0001	0.0013	0.0198	0.0025	0.0058	0.0013
$9/2_1 \to 7/2_1$	0.0045	0.0954	0.0002	0.0015	0.0009	0.0265	0.0003	0.0031
$9/2_2 \to 9/2_1$	0.0000	0.0013	0.0003	0.0040	0.0049	0.0027	0.0010	0.0473
$11/2_1 \to 9/2_1$	0.0019	0.0012	0.0037	0.0041	0.0013	0.1241	0.0002	0.0510
$11/2_2 \to 11/2_1$	0.0003	0.0021	0.0000	0.0010	0.0174	0.0004	0.0012	0.0078
$13/2_2 \to 13/2_1$	0.0002	0.0054	0.0000	0.0179	0.0028	0.0509	0.0001	0.0404
$13/2_1 \to 11/2_1$	0.0013	0.0320	0.0001	0.0004	0.0000	0.0147	0.0003	0.0050

TABLE IX. Calculated $B(E2)$ values (in unit e^2b^2) and $B(M1)$ values (in unit μ_N^2) for $^{91-97}$Y isotopes. The available experimental data is given in the second row.

	^{91}Y		^{93}Y		^{95}Y		^{97}Y	
$j_i^- \to j_f^-$	$B(E2)$	$B(M1)$	$B(E2)$	$B(M1)$	$B(E2)$	$B(M1)$	$B(E2)$	$B(M1)$
$3/2_1 \to 1/2_1$	0.0072	0.0034	0.0110	0.0031	0.0159	0.0030	0.0207	0.0026
				0.0015				
$3/2_2 \to 1/2_1$	0.0111	0.0142	0.0114	0.0124	0.0117	0.0111	0.0121	0.0094
$5/2_1 \to 3/2_1$	0.0016	0.0098	0.0019	0.0105	0.0026	0.0107	0.0030	0.0114
$5/2_2 \to 3/2_1$	0.0088	0.0052	0.0093	0.0046	0.0102	0.0043	0.0099	0.0034
$7/2_1 \to 5/2_1$	0.0028	0.0054	0.0036	0.0048	0.0050	0.0048	0.0057	0.0038
$7/2_2 \to 5/2_1$	0.0015	0.0005	0.0039	0.0005	0.0063	0.0003	0.0113	0.0006
$9/2_1 \to 7/2_1$	0.0039	0.0132	0.0030	0.0142	0.0030	0.0140	0.0020	0.0151
$9/2_2 \to 7/2_1$	0.0040	0.0045	0.0041	0.0042	0.0042	0.0041	0.0043	0.0034
$11/2_1 \to 9/2_1$	0.0030	0.0086	0.0033	0.0076	0.0043	0.0076	0.0042	0.0057
$11/2_2 \to 9/2_1$	0.0000	0.0001	0.0004	0.0000	0.0011	0.0000	0.0029	0.0000
$13/2_1 \to 11/2_1$	0.0062	0.0129	0.0047	0.0145	0.0044	0.0139	0.0025	0.0161
$13/2_2 \to 11/2_1$	0.0025	0.0044	0.0024	0.0042	0.0020	0.0041	0.0022	0.0037

We can analyze the properties of the electric quadrupole ($E2$) and magnetic dipole transitions ($M1$) of odd-odd nuclei using the eigenstate of the IBFFM-1 Hamiltonian. In the present framework, the operator $E2$ and $M1$ take the following forms:

$$\hat{T}(E2) = \hat{T}_B(E2) - \frac{1}{\sqrt{5}} \sum_{\rho=\upsilon,\pi} \sum_{j_\rho j'_\rho} \left(u_{j_\rho} u_{j'_\rho} - \upsilon_{j_\rho} \upsilon_{j'_\rho}\right) \times \langle j'_\rho \| e_{F_\rho} r^2 Y^{(2)} \| j_\rho \rangle \left(a^\dagger_{j_\rho} \times \tilde{a}_{j'_\rho}\right) \quad (22)$$

$$\hat{T}(M1) = \sqrt{\frac{3}{4\pi}} g_b (d^\dagger \times \tilde{d})^{(1)} - \frac{1}{\sqrt{3}} \sum_{\rho=\upsilon\pi} \sum_{j_\rho j'_\rho} \left(u_{j_\rho} u_{j'_\rho} + \upsilon_{j_\rho} \upsilon_{j'_\rho}\right) \times \langle j'_\rho \| g_{l_\rho} I + g_{s\rho} s \| j_\rho \rangle \left(a^\dagger_{j_\rho} \times \tilde{a}^{(1)}_{j'_\rho}\right). \quad (23)$$

The experimental data about the electromagnetic transitions are rather scarce for $^{90-96}$Sr isotopes. The values of parameters α_2 and β_2 in Eq. (17) were searched carefully depending on the experimental transition $B(E2; 2_1^+ \to 0_1^+)$ of the ^{94,96}Sr, the value of α_2 and $\beta_2 = 0.055$ eb for all nuclei. It is noticeable that the $B(E2)$ values of the $2_1^+ \to 0_1^+$, $4_1^+ \to 2_1^+$, and $6_1^+ \to 4_1^+$ transitions increase with increasing in the neutron number. Table VII shows the calculated $B(E2)$ transition rates in comparison with the available data. It seems that the results are good, and consistent with the experimental values.

For odd-A nuclei, the effective charges 1.5 e and 0.5 e are taken for the proton and the neutron, respectively. We used the standard boson g factor values $g_\pi = 1\mu_N$ and $g_\upsilon = 0\mu_N$, while the spin factors g_s value has been quenched by a factor of 0.5 for both proton and neutron, usually lie in the range

TABLE X. Calculated $B(E2)$ values [in unit (e^2b^2)] and $B(M1)$ values (in unit μ_N^2) for $^{92-98}$Y isotopes. The available experimental data is given in the second row.

	^{92}Y		^{94}Y		^{96}Y		^{98}Y	
$j_i^- \to j_f^-$	$B(E2)$	$B(M1)$	$B(E2)$	$B(M1)$	$B(E2)$	$B(M1)$	$B(E2)$	$B(M1)$
$1_1 \to 0_1$		0.4989		0.5028		0.0997		0.0161
						0.0537(1)		0.0961(28)
$2_1 \to 0_1$	0.0056		0.0042		0.0186		0.0239	
					0.0004(1)		>0.0003	
$2_1 \to 1_1$	0.0135	0.0135	0.0119	0.0617	0.0257	0.0654	0.0240	0.0293
					0.0035(18)		0.0003	0.0118
$2_2 \to 2_1$	0.0035	0.0038	0.0108	0.0143	0.0024	0.0151	0.0011	0.0094
					0.0044(1)			
$2_3 \to 2_2$	0.0086	0.0040	0.0014	0.1083	0.0137	0.0001	0.0068	0.0207
$8_1 \to 6_2$	0.0000		0.0017		0.0043		0.0002	
					0.0041(5)			
$2_2 \to 1_2$	0.0011	0.4911	0.0052	0.4548	0.0000	0.0065	0.0004	0.0289
$2_2 \to 3_1$	0.0167	0.0051	0.0002	0.3565	0.0089	0.1738	0.0086	0.0118
$3_1 \to 2_1$	0.0003	0.0518	0.0229	0.0998	0.0079	0.0000	0.0010	0.0039
$3_2 \to 2_1$	0.0049	0.0050	0.0001	0.0040	0.0022	0.0101	0.0170	0.0192
$2_3 \to 2_1$	0.0030	0.0619	0.0007	0.0033	0.0142	0.0289	0.0343	0.0253

$g_s^F/g_s^f \approx 0.4$–0.7 [59–65]. We have used the $g_b = 0.97\,\mu_N$ for all nuclei. The transition probabilities values in Table VIII are somewhat similar in their behavior in the first two isotopes, but they begin to differ at the ^{95}Sr nucleus due to the change in the angular momentum of the ground state. In ^{93}Sr the $3/2_1^+$ state decays to the ground state via a pure $M1$ transition. In the ^{95}Sr isotope, the $5/2_1^+$ and $7/2_1^+$ states are associated with the $\upsilon g_{7/2}$ and $\upsilon d_{3/2}$ orbitals in their wave function configuration, appearing sizable mixing of these two quasiparticle orbitals. Accordingly, these states are connected by strong $M1$ and weak $E2$ transitions. The calculated $B(E2)$ for the $7/2_1^+ \rightarrow 3/2_1^+$ is greater than the experimental $B(E2)$ value. For ^{97}Sr, the $B(M1)$ transitions of $3/2_1^+ \rightarrow 1/2_1^+$ and $5/2_3^+ \rightarrow 3/2_2^+$ in good agreement with experimental value. Another $B(M1)$ transition from $5/2_3^+$ state to $5/2_2^+$ state is equal to [0.0228 and 0.00181(0.0002)] μ_N^2 in (IBFM-1 and EXP) calculations, respectively.

Mostly, all $B(M1)$ transitions in $^{91-97}$Y decrease with increasing mass number and reach the lowest value at the ^{97}Y nucleus. This may be due to the general deformation at the start of the shift to the prolate shape at $N = 59$. From Table IX, it is noticed that there is a slight decrease in the transitions or remain fixed for the ^{93}Y nucleus, after which it begins to decrease gradually to reach the minimum value at the ^{97}Y nucleus.

The properties of the electric quadrupole ($E2$) and magnetic dipole transitions ($M1$) of odd-odd nuclei have been calculated using the eigenstate of the IBFFM-1 Hamiltonian. In Table X, we listed and compared the experimental and calculated electric quadrupole $B(E2)$ and magnetic dipole $B(M1)$ transitions. In the calculation of $B(E2)$ and $B(M1)$, we kept the same value of parameters used in even-even and odd-A nuclei calculations. The experimental transitions data are scarce generally and not available in ^{92,94}Y nuclei. The calculated $B(E2)$ values were generally much larger than the experimental values. Depending on IBFFM-1 calculations in ^{96}Y, the state with $J^\pi = 1_1^-$ decays to the 0_1^- by $B(M1) = 0.0997\,\mu_N^2$ in a good agreement with the experimental data. Moreover, electromagnetic transitions were readily available for the ^{98}Y nucleus. The theoretical values were generally higher than the experimental transition values. The $B(E2;2_2^- \rightarrow 2_1^-) =$ (0.044(10),0.0011) e^2b^2 in experimental and IBFFM-1, respectively. The transitions $B(E2;2_1^- \rightarrow 0_1^-)$ and $B(E2;2_1^- \rightarrow 1_1^-)$ increased continuously with increasing mass number except for a slight decrease for both transitions in ^{94}Y nucleus, this was offset by a significant decrease in the transition $B(M1;1_1^- \rightarrow 0_1^-)$, except for a slight increase at ^{94}Y nucleus.

IV. CONCLUSION

The present boson model calculations give a rather good description of the nuclear structure of even-even $^{90-96}$Sr, odd-A $^{91-97}$Sr, $^{91-97}$Y, and odd-odd $^{92-98}$Y isotopes. The IBFM-1 calculations were carried out with boson-fermion interactions plus fermion Hamiltonian are performed to obtain the positive- and negative-parity energy levels for the odd-A Sr and Y isotopes. The low-lying negative- and positive-parity states of $^{92-98}$Y isotopes are an interesting example of the calculation of the IBFFM to this mass region. A set of levels $J = 1^-$–5^- appears systematically in all isotopes, but the splitting differs in different isotopes. For definite assignments of the positive parity states, more information is required.

Based on the experimental spectrum of ^{96,98}Y, it has been observed that there are 1^+ states below 1 MeV in energy. In our calculation, there is no 1^+ state in that energy range. However, there are eight states in ^{98}Y isotope with $J^+ =$ 3–6, two of them have been observed in the experimental spectrum. These states may play an important role in understanding the properties and behavior of this nucleus, and further investigation is necessary to fully understand their characteristics and significance. Although deformed states of ^{96,98}Y can be obtained in IBFFM using an SU(3) boson term, the computations required for treating the deformed states would be prohibitively large. This is because it would involve the full valence oscillator shells for protons and neutrons. Although the experimental data about the $B(E2)$ and $B(M1)$ values are rather scarce or not available for some isotopes. However, the present model calculations of transition probabilities will serve as a motivation for the experimentalists to work for the identification of these values. We demonstrated that the negative-parity states in odd-Sr isotopes could be described using $h_{11/2}$ and next shell configurations. On the other hand, by including the $d_{5/2}$ configuration for the following shell, positive-energy states in odd-Y isotopes are likely to be produced. Therefore, while IBFFM can be used to predict some properties of heavier isotopes, further methods and computations may be necessary to fully understand the coexistence of spherical and deformed phases in these nuclei.

ACKNOWLEDGMENT

The authors would like to thank Prof. A. R. Subber for his interest in the subject and his many helpful suggestions.

[1] K. Heyde and J. L. Wood, Rev. Mod. Phys. **83**, 1467 (2011).
[2] C. Sotty, Coulomb excitation of neutron-rich Rb isotopes around $N = 60$; Production of nuclear spin polarized beams using the Tilted Foils technique, Ph.D. thesis, Université Paris Sud-Paris XI, 2013.
[3] J. L. Wood and K. Heyde, J. Phys. G: Nucl. Part. Phys. **43**, 020402 (2016).
[4] V. Manea, D. Atanasov, D. Beck, K. Blaum, C. Borgmann, R. Cakirli, T. Eronen, S. George, F. Herfurth, and A. Herlert, Phys. Rev. C **88**, 054322 (2013).
[5] A. Esmaylzadeh, J. M. Régis, Y. H. Kim, U. Köster, V. Karayonchev, L. Knafla, K. Nomura, L. Robledo, and R. Rodríguez-Guzmán, Phys. Rev. C **100**, 064309 (2019).

[6] B. Cheal, M. Gardner, M. Avgoulea, J. Billowes, M. Bissell, P. Campbell, T. Eronen, K. Flanagan, D. Forest, and J. Huikari, Phys. Lett. B **645**, 133 (2007).

[7] U. Hager, A. Jokinen, V. Elomaa, T. Eronen, J. Hakala, A. Kankainen, S. Rahaman, J. Rissanen, I. Moore, and S. Rinta-Antila, Nucl. Phys. A **793**, 20 (2007).

[8] T. Hagen, A. Görgen, W. Korten, L. Grente, M. Salsac, F. Farget, I. Ragnarsson, T. Braunroth, B. Bruyneel, and I. Celikovic, Phys. Rev. C **95**, 034302 (2017).

[9] S. Rinta-Antila, S. Kopecky, V. S. Kolhinen, J. Hakala, J. Huikari, A. Jokinen, A. Nieminen, J. Äystö, and J. Szerypo, Phys. Rev. C **70**, 011301 (2004).

[10] J. Hakala, R. Rodríguez-Guzmán, V. Elomaa, T. Eronen, A. Jokinen, V. S. Kolhinen, I. D. Moore, H. Penttilä, M. Reponen, J. Rissanen, A. Saastamoinen, and J. Äystö, Eur. Phys. J. A **47**, 129 (2011).

[11] L. J. Vormawah, M. Vilén, R. Beerwerth, P. Campbell, B. Cheal, A. Dicker, T. Eronen, S. Fritzsche, S. Geldhof, A. Jokinen, S. Kelly, I. D. Moore, M. Reponen, S. Rinta-Antila, S. O. Stock, and A. Voss, Phys. Rev. A **97**, 042504 (2018).

[12] M. Akbari and A. Kardan, Nucl. Phys. A **990**, 109 (2019).

[13] H. Abusara and S. Ahmad, Phys. Rev. C **96**, 064303 (2017).

[14] D.-L. Zhang and C.-F. Mu, Chin. Phys. Lett. **33**, 102102 (2016).

[15] H. Wollnik, F. K. Wohn, K. D. Wünsch, and G. Jung, Nucl. Phys. A **291**, 355 (1977).

[16] N. Warr, E. Clément, M. Albers, D. Balabanski, V. Bildstein, A. Blazhev, J. Cederkäll, J.-M. Daugas, T. Davinson, G. Georgiev, R. Gernhäuser, A. Görgen, D. Jenkins, J. Jolie, W. Korten, T. Kröll, R. Krücken, J. Ljungvall, R. Lozeva, N. Mărginean, D. Mücher, A. Obertelli, J. Pakarinen, P. Reiter, M. Scheck, M. Seidlitz, S. Siem, G. Simpson, D. Voulot, F. Wenander, K. Wimmer, and P. Woods, European Organization for Nuclear Resarch CERN-INTC-027/INTC-I-096 (2010).

[17] E. H. Wang, J. H. Hamilton, A. V. Ramayya, R. Han, C. J. Zachary, J. M. Eldridge, J. K. Hwang, N. T. Brewer, Y. X. Luo, J. O. Rasmussen, S. J. Zhu, G. M. Ter-Akopian and Y. T. Oganessian, Int. J. Mod. Phys. E **27**, 1850051 (2018).

[18] E. Tel, M. Sahan, H. Sahan, H. Alkanli, and Y. Kavun, AIP Conf. Proc. **2042**, 020058 (2018).

[19] E. Clément, M. Zielińska, Phys. Scr. **92**, 084002 (2017).

[20] K. Nomura, R. Rodríguez-Guzmán, and L. M. Robledo, Phys. Rev. C **94**, 044314 (2016).

[21] J.-M. Régis *et al.*, Phys. Rev. C **95**, 054319 (2017).

[22] K. Wimmer *et al.*, European Organization for Nuclear Research CERN-INTC-055/INTC-I-237 (2021).

[23] S. Cruz *et al.*, Phys. Rev. C **100**, 054321 (2019).

[24] K. Sieja, Universe **8**, 23 (2022).

[25] S. Cruz *et al.*, Phys. Rev. C **102**, 024335 (2020).

[26] H. Mei, J. Xiang, J. M. Yao, Z. P. Li, and J. Meng, Phys. Rev. C **85**, 034321 (2012).

[27] A. Arima and F. Iachello, Ann. Phys. (NY) **99**, 253 (1976).

[28] A. Arima and F. Iachello, Ann. Phys. (NY) **111**, 201 (1978).

[29] A. Arima and F. Iachello, Ann. Phys. (NY) **123**, 468 (1979)

[30] F. Iachello and O. Scholten, Phys. Rev. Lett. **43**, 679 (1979).

[31] O. Scholten and A. E. L. Dieperink, in *Interacting Bose-Fermi Systems in Nuclei*, edited by F. Iachello (Plenum Press, New York, 1981).

[32] S. Brant, V. Paar, and D. Vretenar, Z. Phys. A **319**, 355 (1984).

[33] A. Balantekin and V. Paar, Phys. Lett. B **169**, 9 (1986).

[34] P. Van Isacker, J. Jolie, K. Heyde, and A. Frank, Phys. Rev. Lett. **54**, 653 (1985).

[35] K. Nomura, R. Rodríguez-Guzmán, and L. M. Robledo, Phys. Rev. C **101**, 014306 (2020).

[36] R. F. Casten and D. D. Warner, Rev. Mod. Phys. **60**, 389 (1988).

[37] F. Iachello and P. Van Isacker, *The Interacting Boson-Fermion Model* (Cambridge University Press, Cambridge, 1991).

[38] J. Bardeen, N. L. Cooper, and J. R. Schrieffer, Phys. Rev. **108**, 1175 (1957).

[39] W. T. Chou, W. C. McHarris, and O. Scholten, Phys. Rev. C **37**, 2834 (1988).

[40] D. Bucurescu, C. A. Ur, M. Ionescu-Bujor, A. Iordăchescu, D. Bazzacco, F. Brandolini, G. de Angelis, M. De Poli, A. Gadea, S. Lunardi, N. Mărginean, N. H. Medina, D. R. Napoli, P. Pavan, C. Rossi Alvarez, and P. Spolaorec, Nucl. Phys. A **705**, 3 (2002).

[41] O. Scholten, IBFFM code, 1988 (unpublished).

[42] S. Brant and V. Paar, Z. Phys. A - Atomic Nucl. **329**, 151 (1988).

[43] ENSDF, Nuclear data Sheet (2023), http://www.nndc.bnl.gov/ensdf.

[44] G. L. Long, Z. Jinyu, and T. Lin, Commun. Theor. Phys. **29**, 249 (1998).

[45] E. A. Stefanova, M. Danchev, R. Schwengner, D. L. Balabanski, M. P. Carpenter, M. Djongolov, S. M. Fischer, D. J. Hartley, R. V. F. Janssens, W. F. Mueller, D. Nisius, W. Reviol, L. L. Riedinger, and O. Zeidan, Phys. Rev. C **65**, 034323 (2002).

[46] K. Heyde, J. Jolie, J. Moreau, J. Ryckebusch, M. Wsroquier, P. Van Duppen, M. Huyse, and J. L. Wood, Nucl. Phys. A **466**, 189 (1987).

[47] M. Biischer, R. F. Casten, R. L. Gill, R. Schuhmann, J. A. Winger, H. Mach, M. Moszynski, and K. Sistemich, Phys. Rev. C **41**, 1115 (1990).

[48] L. S. Kisslinger and R. A. Sorensen, Rev. Mod. Phys. **35**, 853 (1963).

[49] S. Brant, G. Lhersonneau, V. Paar, and K. Sistemich, Z. Phys. A - Atomic Nucl. **333**, 1 (1989).

[50] R. A. Meyer, Hyperfine Interact. **22**, 385 (1985).

[51] G. Lhersonneau, B. Pfeiffer, K. L. Kratz, H. Ohm, K. Sistemich, S. Brant, and V. Paar, Z. Phys. A - Atomic Nucl. **337**, 149 (1990).

[52] O. Scholten, Prog. Part. Nucl. Phys. **14**, 189 (1985).

[53] D. Bucurescu, G. Căta-Danil, N. V. Zamfir, A. Gizon, and J. Gizon, Phys. Rev. C **43**, 2610 (1991).

[54] G. Căta-Danil, D. Bucurescu, A. Gizon, and J. Gizon, J. Phys. G **20**, 1051 (1994).

[55] C. E. Alonso, J. M. Arias and Lozano, J. Phys. G **13**, 1269 (1987).

[56] S. Brant, K. Sistemich, H. Seyfarth, H. Ohm, M. L. Stolzenwald, V. Paar, D. Vretenar, D. Vorkapi, V. Lopac, R. A. Meyer, G. Lhersonneau, K.-L. Kratz, and B. Pfeiffer, *Nuclear Structure of the Zirconium Region* (Springer-Verlag, Berlin, 1988).

[57] B. Singh and Z. Hu, Nucl. Data Sheets **98**, 335 (2003).

[58] S. Brant, G. Lhersonneau, and K. Sistemich, Phys. Rev. C **69**, 034327 (2004).

[59] F. H. Al-Khudair, Phys. Rev. C **91**, 054304 (2015).

[60] A. Bohr and B. R. Mottelson, *Nuclear Structure*, V.2 (World Scientific, Singapore, 1998).

[61] N. Yoshida, L. Zuffi, and S. Brant, Phys. Rev. C **66**, 014306 (2002).

[62] S. Brant, N. Yoshida, and L. Zuffi, Phys. Rev. C **70**, 054301 (2004).
[63] L. Zuffi, S. Brant, and N. Yoshida, Phys. Rev. C **68**, 034308 (2003).
[64] F. H. Al-Khudair, G. L. Long, and Y. Sun, Phys. Rev. C **77**, 034303 (2008).
[65] J. Rikovska, N. J. Stone, P. M. Walker, and W. B. Walters, Nucl. Phys. A **505**, 145 (1989).